Reviewed Preprint
v1 • June 5, 2025
Not revised

Reviewed Preprint
v2 • July 16, 2026
Revised by authors

For correspondence:
jenny.wang@cs.ox.ac.uk

Competing interests: No competing interests declared

Funding: See page 35

Reviewing editor: Patrick M Boyle, University of Washington, United States

Calibration and validation strategy for electromechanical cardiac digital twins

Zhinuo Jenny Wang[1], Maxx Holmes[1], Ruben Doste[1], Julia Camps[1], Francesca Margara[1], Mariano Vazquez[2,3], Blanca Rodriguez[1]

[1]Department of Computer Science, University of Oxford, Oxford, United Kingdom • [2]Barcelona Supercomputing Centre, Barcelona, Spain • [3]ELEM Biotech, Barcelona, Spain

eLife Assessment

This study offers an **important** set of literature-based parameter ranges for calibrating cardiac electromechanical models. The key scientific claims are largely supported by **convincing** evidence and carefully-documented methodologies, but a few specific issues remain only partially supported, in particular relating to the locking-free formulation, reporting of adequate details regarding the electrophysiological model (Eikonal approach), and the fact that physiological accuracy is predominantly achieved in a single chamber (the LV).

https://doi.org/10.7554/eLife.106555.2.sa3

Abstract

State-of-the-art cardiac electromechanical modelling and simulation form the basis for recent developments in cardiac Digital Twin technologies. However, a comprehensive evaluation of electromechanical models at cellular, tissue, and organ level has yet to be performed that addresses both ECG and pressure-volume biomarkers. Such an evaluation would build credibility for applications of cardiac Digital Twins in clinical research and therapy development.

We aimed to follow ASME V&V40 standards for calibration, validation, and sensitivity analysis of ventricular electromechanical models under healthy conditions, to progress towards the Digital Twin vision. We performed a multi-scaled review of ventricular electromechanics and compiled a dataset for calibration and validation incorporating ECG, pressure-volume, displacement, and strain biomarkers.

When applied to a biventricular multiscale model, we achieved healthy calibrated values for the QRS duration (89 ms), QT interval (360 ms), left ventricular ejection fraction (LVEF) (51 %), peak systolic pressure (14 kPa), end diastolic (105 mL) and end systolic volumes (51 mL), peak ejection flow rate (180 mL/ms). Model validation was performed by comparison to displacement and strain biomarkers including systolic atrioventricular plane displacement (1.5 cm), systolic fibre strain (−0.18) and longitudinal strain (−0.15). Sensitivity analysis of model parameters at cellular and ventricular scales was also performed to inform model calibration and as a first step towards uncertainty quantification. We quantified the effects of variability in ionic conductance, mechanical stiffness, cross-bridge cycling dynamics, and systemic circulation on action potential and active tension dynamics at the cellular scale, and on ECG, pressure-volume, displacement, and strain biomarkers at the ventricular scale. Simulations showed that the relationship between healthy LVEF and T wave biomarkers was primarily underpinned by variability in L-type calcium channel conductance and SERCA activity through multi-scale effects. In this study, we provide a systematic framework for credibility assessment of cardiac electromechanical models based on both ECG and mechanical biomarkers, as a foundational step towards the cardiac Digital Twin vision.

Introduction

Digital Twins are expected to play an increasingly important role in healthcare to enable tailored therapy design for precision medicine. The importance of this emerging technology was attested to by recent regulatory attention and the publication of the ASME V&V40 Standard in 2018[1]. The Standard provided a risk-based framework for evaluating their credibility for biomedical applications. A cardiac digital twin is envisioned as a patient-specific computational model of the heart, personalised from multi-modal clinical data and continuously updated to support diagnosis, prognosis, and treatment planning[2–4]. This is a goal that no published cardiac electromechanical study has yet simultaneously fulfilled, and towards which credible, systematically validated models are an essential first step.

At the core of the cardiac Digital Twin are realistic high-fidelity mechanistic models that can coherently assimilate multi-modal and multi-scale data and can explain disease mechanisms and predict therapy outcomes[5–7]. An important aspect of cardiac function is the coupling of electrophysiology and mechanics in the ventricles[8–10]. To describe electromechanical function, multiscale, mechanistic models are built on mathematical descriptions of electromechanical coupling at cellular, tissue, and organ scales. The biophysical detail gives the model the advantage of high explainability and predictive power over statistical or machine learning approaches. Electromechanical cardiac models have had broad applicability in cardiology, such as in unravelling the relationship between the electrocardiogram (ECG) and mechanical deformation[11], the ECG and ejection fraction in post-myocardial infarction[12], demonstrate how mechanical deformation provides triggers and substrate for arrhythmia[13] and affects re-entrant wave stability[14], and predicting therapy outcomes in hypertrophic cardiomyopathy[15] and heart failure[16]. Recent developments towards the Digital Twin vision have enabled increasingly personalised models through assimilation of omics, imaging, blood pressure, and electrocardiogram (ECG) data[9,17–19] and promises to deliver patient-specific therapy planning[20] in the near future.

Despite significant developments, a lack of thorough reviews of model credibility considering both electrophysiological and mechanical properties from cell to organ scales hinders wider progress acceptance and impact of cardiac Digital Twins. Thus far, cardiac applications of the ASME V&V40 standards have focused on device optimisation using fluid-structure interaction models for left ventricular assistive devices[21] and for artificial heart valves[22], but this has yet to be applied to ventricular electromechanical simulations. Examples of rigorous model evaluation at cellular scale[23–25] highlight the importance of strictly separating calibration and validation data[23] and consideration of both electrophysiological and mechanical biomarkers[26]. At the ventricular scale, most studies focused either on the ECG[11] or pressure-volume biomarkers[27–30,21,31] but not on both, and deformation and strain biomarkers are rarely considered. Simulation studies have investigated how model parameters relate to specific aspects of cardiac electromechanical function, such as the atrioventricular plane displacement[31], and how model deformations relate to ECG morphologies[11], but not in a comprehensive manner. Large scale global sensitivity analyses studies of pressure and volume biomarkers have analysed effects from anatomical variations[28] and contractility and haemodynamic parameter variations[32], without any analysis of concurrent ECG biomarker effects. Furthermore, the strategies and data used for calibration and validation in these studies were typically not discussed[8,9,28]. In particular, while Camps et al.[33] demonstrated personalised ECG calibration in a purely electrophysiological framework, and Strocchi et al.[32] performed global sensitivity analysis of pressure-volume biomarkers in a whole-heart model, neither study examined the concurrent influence of cellular, mechanical, and haemodynamic parameters on both ECG and pressure-volume characteristics within a single coupled electromechanical framework.

Therefore, in this study we aim to propose a calibration and validation strategy, which starts with gathering the required experimental and clinical dataset for model parameters and simulation outcomes, and considering both ECG and mechanical biomarkers for the evaluation of high-fidelity ventricular electromechanical cardiac models, as the foundation towards the Digital Twin

vision. We then apply ASME V&V40 principles to a multiscale, biventricular electromechanical model with clinical image-based anatomy and realistic ECG, with the aim to 1) reproduce healthy pressure-volume, ECG, deformation, and strain dynamics, and 2) investigate multi-scale mechanisms that underpin the relationship between ECG and pressure-volume biomarkers.

Materials and methods

This study is structured in two parts, following ASME V&V40 principles. First, we establish a general framework for calibration, validation, and sensitivity analysis of ventricular electromechanical models, comprising a systematic review of biomarkers spanning cellular, tissue, and organ scales, and their organisation into non-overlapping calibration and validation sets. Second, we demonstrate this framework through a specific example, applying it to a state-of-the-art biventricular electromechanical model under healthy conditions. This two-part structure is intentional: the framework is designed to be reusable and applicable to any electromechanical model and dataset, while the specific example provides a transparent evaluation of current modelling capability with consideration of both electrophysiological and mechanical biomarkers.

Model assessment strategy

Following examples of the ASME V&V 40-based analysis applied in the context of cardiovascular science [21,34], we devised a calibration and validation strategy for human ventricular electromechanical modelling and simulation frameworks by considering the following:

Question of interest

Can the modelling and simulation framework produce healthy physiological electromechanical function at cellular, tissue, and organ levels including both ECG and pressure-volume loop biomarkers?

Context of use

Human ventricular electromechanics models provide mechanistic explanations for various disease conditions and evaluate therapeutic interventions. Here we focused on model evaluation under healthy conditions to build the foundations of model credibility for disease and therapy investigations in the future.

Quantities of interest

To ensure model relevance to its context of use, the quantities of interest were chosen to be biomarkers with known links to key cardiac diseases, including Torsade de Pointes, myocardial infarction, hypertrophic cardiomyopathy, dilated cardiomyopathy, heart failure, and pulmonary hypertension. Therefore we selected the following biomarkers from the 12-lead ECG (QRS duration, QT dispersion, T wave amplitude, T peak to T end duration, and JT interval), the pressure-volume relationship (left and right end diastolic and end systolic volumes and end systolic pressures, and left ejection fraction, left pressure upstroke velocity, left peak ejection and peak filling flow rate), and from measurements of displacement (end diastolic and end systolic wall thicknesses, atrioventricular plane displacements, systolic percentage volume change, and apical displacement) and strain (systolic global longitudinal strain, radial strain, circumferential strain, and fibre stretch ratio). The specific relevance of each biomarker to cardiac diseases was summarised (Table 2, Results).

Cellular biomarkers including action potential duration (APD90), active tension peak (Ta_{max}), active tension duration (TaD50) and peak upstroke of active tension (dTa/dt_{max}) were not explicitly included in the biomarker list since they have already been used to calibrate and validate the cellular electromechanical model previously[23,26]. However, these properties were evaluated in sensitivity analyses (see below) to inform ventricular simulations.

Group	Parameters	Initial value	Literature ranges	Ranges for sensitivity analysis
Passive mechanics parameters	a, af, as, afs	0.61 kPa, 1.56 kPa, 0.70 kPa, 0.46 kPa	0.61, 1.56, 0.70, 0.46 kPa (fitted to human data shear and axial data)[38] 0.057, 21.503, 6.841,- kPa (fitted to partial shear pig data)[39] 0.059, 18.472, 2.481, 0.216 kPa (fitted to full shear pig data)[39] 2.28, 1.685, -, - kPa (fitted to biaxial dog data)[39] 0.333, 18.535, 2.564, 0.417 kPa [40]29/04/2026 08:20:00 AM	[0.057, 0.61] [1.56, 2.15] [0.7, 6.8410] [0.216, 0.46]
	b, bf, bs, bfs	7.5, 35.31, 33.24, 5.09	7.5, 35.31, 33.24, 5.09 (fitted to human data shear and axial data)[38] 8.094, 15.819, 6.959, - (fitted to partial shear pig data)[39] 8.023, 16.026, 11.12, 11.436 (fitted to full shear pig data)[39]; 9.726, 15.779, -, - (fitted to biaxial dog data)[39] 9.242, 15.972, 10.446, 11.602 [40]29/04/2026 08:20:00 AM	-
	Kct	5000 kPa	3333[40], 10 - 1000 [41]	[10, 5000]

Table 1. Initial parameter values and literature basis for the choice of variability ranges for the model inputs.

Unless stated explicitly, quoted values from the literature have come from previous modelling choices.

Active tension parameters	Tref	120 kPa * 10	120 (fitted to human contraction data)[24]	[1200, 2400]
	Cross-fibre contraction	30% of Tref	0 – 60% [10], 46% (rabbit heart tissue measurements) [42]	-
Pressure volume control parameters	R_LV	10 kPa ms/mL	10 – 100 kPa ms/mL [10] , 100 kPa ms /mL[40], 114 kPa ms/mL [24]	[10, 110]
	R_RV	33.3 kPa ms/mL	A third of left ventricular value [24], 2.0 +- 0.8 mmHg min/L (control patient measurements) [43]	-
	C_LV	1.5 mL/kPa	1.5 mL/ kPa[40], 20.5 mL/kPa[24]	[1.5, 20]
	C_RV	4.5 mL/kPa	Threefold of left ventricular value[24]	-
	P ejection LV	10 kPa	9.7 -10.4 kPa (human measurements)[44], 9 kPa[24]29/04/2026 08:20:00 AM	[9, 10]
	P ejection RV	2.3 kPa	2.3 +- 1 kPa (control patient measurements)[43], 3 kPa[24]	-
	P diastolic cut-off LV	1.3 kPa	1.3 [0.93-1.73] kPa (control patient measurements)[45], 0.1 kPa[24]	-
	P diastolic cut-off RV	1.5 kPa	1.91 ± 0.8 kPa, pulmonary diastolic pressure[43]	-
	Atrial filling duration LV	150 ms	~150 ms at resting cycle length 1000 ms (human exercise measurements)[46]	-
	EDP_LV	1.3 kPa	1.3 ± 0.1 kPa (control patient measurements)[47], ~1 kPa(control patient measurements)[48], 1 kPa[24].	-
	EDP_RV	1.0 kPa	11.0 ± 6.3 mmHg[43], A third of left ventricular value[24]	-
Pericardial constraint	K_epi	500 kPa/cm	20 kPa/cm with 5e-2 kPa*s/cm for viscous term[49], 500 kPa/cm[31], 0 – 100 kPa/cm (20 kPa/cm specifically for baseline)[10]	[20, 500]
Microstructure	Transmural fibre angle endo to epi	-60 to 60 in LV, 90 to –25 in RV, 0	-60 to 60 in LV, 90 to –25 in RV, 0 to 90 at outflow tract[50]	-

Table 1. (continued)

		to 90 at outflow tract		
	Transmural sheet angle to radial axis	0 degrees	-45 endocardium to 45 epicardium (canine measurements) [51], 45 endocardium to 0 epicardium (canine measurements) [52], ~45 degrees at diastole, ~0 degrees at systole (swine DTI measurements)[53]	-
Heart rate	Cycle length	1000 ms	63+-2 beats/min[54], 72 +- 13 beats/min[55]	-

Table 1. (continued)

Calibration dataset				
Group	**Biomarker**	**Ranges**	**Data info**	**Implication for cardiac diseases**
12-lead ECG	JT interval (ms)	313 [294, 335]$_{IQR}$[59]	mixed sex, UKBB CMR, n=76,266	In patients with QRS > 120 ms, risk of Torsade de Pointes[60,61]
	Tpe (ms)	62 (12)$_{IQR}$ [62]	mixed sex, UKBB without life threatening arrhythmias, n=51,574	Risk of SCD[63]
	T wave amplitude (Tpeak) (mV)	0.15 [0.11, 0.19]$_{IQR}$ [7]	mixed sex, UKBB normal ventricular mass, n=36,956	Risk of SCD in HCM[64]
	QT dispersion (ms)	56.6 [37.0, 84.0]$_{IQR}$ [7]	mixed sex, UKBB normal ventricular mass, n=36,956	Severity of CAD[65]
	QRS duration (ms)	89 [81, 97]$_{IQR}$ [7]	mixed sex, UKBB normal ventricular mass, n=36,956	Poor prognosis in DCM[66] and risk

Table 2. Experimental and clinical datasets for calibration of healthy ventricular electromechanical models, with summary of why each biomarker was important due to their implications in cardiac diseases.

Data were presented in the forms: [x, y]95% were 95% confidence intervals, x±ystd were mean and standard deviations, x±zsem were mean and standard error of the mean, [x, y]range were the minimum (x) and maximum (y), x [y, z]IQR were median (x) and first (y) and third (z) quartiles , x (y)IQR were median (x) and interquartile range (y). UKBB indicates values extracted from the UK Biobank. Unit conversions from original source has been done where appropriate to preserve consistency across the entire table. SCD: sudden cardiac death, HCM: hypertrophic cardiomyopathy, DCM: dilated cardiomyopathy, CAD: coronary artery disease, HF: heart failure, HFpEF: HF with preserved ejection fraction, PAH: pulmonary artery hypertension, MI: myocardial infarction, HHD: hypertensive heart disease, LV: left ventricle, RV: right ventricle, EDV: end diastolic volume, ESV: end systolic volume, SVL: stroke volume in left ventricle, SVR: stroke volume in right ventricle, ESP: end systolic pressure, CMR: cardiac magnetic resonance imaging.

				stratification for HFpEF[66]
Pressure volume	LVEDV (mL)	$[88, 161]_{95\%}$ [35]	female UKBB CMR, n=804	Predictor of exercise capacity in HFpEF[67]
	LVESV (mL)	$[31, 68]_{95\%}$ [35]	female UKBB CMR, n=804	Predictor of HFpEF[68]
	RVEDV (mL)	$[85, 166]_{95\%}$ [35]	female UKBB CMR, n=804	Predictor of functional class in PAH[69]
	RVESV (mL)	$[27, 77]_{95\%}$ [35]	female UKBB CMR, n=804	Stratifies PAH[70,71]
	SVL (mL)	$[49, 100]_{95\%}$ [35]	female UKBB CMR, n=804	Incident rate of HF[52]
	LVESP (kPa)	$16.7 \pm 2.2_{std}$ [72]	mixed sex, UKBB, n=150	Associated with hypertrophy[72,73]
	RVESP (kPa)	$3.2 \pm 0.4_{std}$ [74]	male, radionuclide ventriculography, n=12	Stratifies PAH[70,71]
	LVEF (%)	$[51, 70]_{95\%}$ [35]	female UKBB CMR, n=804	Stratifies HF, MI, and SCD risk[75]
	dP/dt_{max} (kPa/s)	$150 \pm 30_{std}$ [76]	catheter measurement in successful CRT, n=17	Surrogate measure of ventricular contractility in HF[77]
	Peak ejection rate (PER) (mL/s)	$410 \pm 102_{std}$ [78]	mixed sex, 3D echocardiography, n=15	Valvular regurgitation[79] and peak systolic velocity associated with CHD[80]
	Peak early filling rate (PFR) (mL/s)	$361 \pm 110_{std}$ [78]	mixed sex, 3D echocardiography, n=15	Points to relaxation dysfunction in CHF[81]

Table 2. (continued)

Compilation of biomarker data

The healthy ranges for each quantity of interest (biomarker) were compiled from the literature. Reports from larger datasets were preferred for better estimates of population variability. For this reason, values were preferentially included from the UK Biobank, which is a large-scale biomedical database with health information from half a million UK participants, with more than 40,000 cardiac magnetic resonance recordings available[35–37]. This is then supplemented by smaller studies as needed. The use of gold standard magnetic resonance imaging data was preferentially included over other imaging modalities such as echocardiography for volumetric and deformation biomarkers.

Separation of calibration vs validation data

The quantities of interest were separated into a calibration and a validation dataset[23]. The calibration dataset consisted of ECG and pressure-volume biomarkers that clinically defined healthy electromechanical function, while the validation dataset included displacement and strain biomarkers that explored the model's capabilities for providing mechanistic explanations.

Sensitivity analyses towards uncertainty quantification

The model was further validated through sensitivity analyses. To showcase versatility, a wider set of parameters were included in the analyses than has explicitly been linked to any disease or therapeutic target. By varying parameters over biologically informed ranges derived from population variability in the literature, the sensitivity analyses characterise how uncertainty in model inputs propagates to uncertainty in simulated biomarkers, providing a foundation for future formal uncertainty quantification using probabilistic inference approaches.

The following model parameters were included from the cellular electrophysiology (conductances of the fast sodium current GNa, late sodium current GNaL, L-type calcium current GCaL, transient outward potassium current Gto, rapid delayed rectifier potassium current GKr, slow delayed rectifier potassium current GKs, sodium calcium exchanger GNCX, inward rectifier current GK1, sodium-potassium pump current GNaK, peak calcium release Jrel, peak calcium re-uptake SERCA, and magnitude of the stimulus current Istim), the cellular active tension generation (peak active tension T_{ref}, calcium sensitivity Cal50, cross bridge transition rates from unbound to pre-powerstroke k_{uw} and from pre- to post-powerstroke k_{ws}), passive mechanical properties (bulk stiffness a, fibre stiffness a_f, sheet stiffness a_s, fibre-sheet shear stiffness a_{fs}, compressibility coefficient Kct, pericardial constraint stiffness K_{epi}), and circulatory haemodynamics (aortic resistance R_{LV}, aortic compliance C_{LV}, aortic ejection threshold pressure $P_{ejectionLV}$).

A review of the literature produced a list of initial model parameter values and their known variabilities (summarised in Table 1). Cellular conductances were uniformly varied from 50 to 200% to cover the experimentally measured ranges as done in previous studies[25]. For passive mechanics, only the parameters carrying units of stiffness were included in the exploration and their initial values were extracted from the non-viscoelastic version of the model fitted to human ex vivo stress-strain measurements[38] and their ranges extracted from literature. The compressibility parameter (Kct), pericardial constraint stiffness (Kepi), and the active tension coefficient (Tref) parameters were allowed greater ranges of variation since they do not correspond to experimental measurements and their physical meanings were model-dependent. Similarly, the resistance and compliance parameters and the ejection threshold pressure were allowed a large variability range since they were part of a lumped parameter model and do not directly map to experimental measurements.

A specific example: human biventricular electromechanical model construction, calibration, validation and sensitivity analysis

Input data

To demonstrate our strategy, we selected a fully covered biventricular tetrahedral mesh with valvular plugs from the publicly available Rodero et al. database[28] (female, age 49, weight 90 kg). A fully covered ventricular geometry, extending from apex to atrioventricular plane without

truncation, was a prerequisite for applying physiologically realistic basal boundary conditions.

Although four-chamber meshes were available, atrial geometry was excluded to ensure applicability to the most common clinical imaging scenario: cardiac MRI, in which atrial walls cannot typically be faithfully reconstructed. The tools and workflows used to apply the framework to this mesh are openly available at *https://github.com/jennyhelyanwe/Cardiac-Electromechanics-Workflow*, while the ECG calibration code is based on *https://github.com/juliacamps/Cardiac-Digital-Twin*, enabling other researchers to apply the same framework to their own patient-specific geometries and datasets.

Since the mesh was constructed based on imaging data at end diastole, the mesh was scaled down isotropically to achieve a diastasis volume of 80 mL[43] to mimic the process of unloading to diastasis. Fibre f_0, sheet s_0, and sheet-normal n_0 vectors at resting were generated using a rule-based method designed for biventricular geometry with outflow tracts[50]. Ventricular coordinates were taken from the published database[28], and consisted of the longitudinal coordinate (uvc_l) where uvc_l = 1 at the apex and 0 at the base, a transmural coordinate (uvc_t), where endocardium was uvc_t = 1 and epicardium was uvc_t = 0, and a rotational coordinate (uvc_r), where uvc_r = 0 was in the middle of the left ventricular lateral wall.

Human electrophysiological model

Simulation of the electrical excitation and relaxation through the ventricles was through the monodomain model with orthotropic diffusion along the fibre, sheet, and sheet-normal directions. Ionic current dynamics and calcium handling dynamics were modelled using the human ventricular electrophysiological cell ToR_ORd model [23], with extensive validation on experimental action potential morphology and calcium dynamics, as well as responses to multi-channel drug block.

Purkinje-myocardial junctions were modelled using a fast endocardial activation layer with isotropic conduction velocity σ_{endo} on the left and right ventricular endocardial surfaces. Standard 12-lead electrode positions were manually mapped from the heart and torso geometry of a previous study to the current geometry, and the 12-lead ECG was simulated at these electrode positions using the pseudo-ECG method[18].

Mechanical model

The mechanical behaviour was characterised by the balance of linear momentum in a total Lagrangian formulation, considering inertial contributions but ignoring volumetric forces. The reference configuration was the scaled down version of the biventricular mesh (diastasis) $\Omega_0 \subset R^3$, at t = 0. The constitutive law for the passive mechanical behaviour of the ventricular tissue was a nearly incompressible version of Holzapfel and Ogden which was orthotropic in mechanical behaviour[10]. The strain energy density function defining this hyper-elastic continuum is:

$$\psi(C) = \frac{K_{ct}}{2}(J-1)^2 + \frac{a}{2b}\left(e^{b(\bar{I}_1-3)}-1\right) + \sum_{i=f,s}\frac{a_i}{2b_i}\left(e^{b_i(\bar{I}_{4i}-1)^2}-1\right) + \frac{a_{fs}}{2b_{fs}}\left(e^{b_{fs}\bar{I}_{8fs}^2}-1\right)$$

where $J = det(F)$, $C = F^TF$, bar notation indicates that $\bar{x} = J^{\frac{-2}{3}}x$, f_0 and s_0 indicate fibre and sheet directions, respectively, in the reference configuration such that $I_1 = trC$, $I_{4f} = f_0 Cf_0$, $I_{4s} = s_0 Cs_0$, $I_{8fs} = \frac{1}{2}(f_0 Cs_0 + s_0 Cf_0)$, and K_{ct} controls the compressibility of the material. The reader is directed elsewhere[10] for the precise form of the passive contribution to the second Piola-Kirchhoff stress tensor.

Boundaries were defined as: epicardium Γ_{epi}, left ventricular endocardium Γ_{LVendo}, right ventricular endocardium Γ_{RVendo}, and the epicardial surface Γ_{epi},

$$\begin{aligned} FSn_0 - JP_{LVendo}F^{-T}n_0 &= 0, \text{on}_{\text{LVendo}} \times (0,T], \\ FSn_0 - JP_{RVendo}F^{-T}n_0 &= 0, \text{on}_{RVendo} \times (0,T], \\ FSn_0 - (K_{epi}(uvc_l)\, u \cdot n_0)\, n_0 &= 0, \text{on}_{epi} \times (0,T] \end{aligned}$$

where n_0 was the outward normal defined on the whole material boundary $\partial\Omega_0$, and $K_{epi}(uvc_l)$ was the stiffness corresponding to an elastic spring boundary condition applied to the endocardium and was described as a step function of the longitudinal coordinate l with magnitude of K_{epi} at values of $0 < uvc_l < 0.85$ (i.e. applied for 85% of the longitudinal dimension of the heart from the apex). This was a simplified version of the method[31], which fitted image-derived epicardial displacement to fit a normalised penalty scale that went from 1 from the apex to mid-ventricle, and transitioned through a sigmoidal function to 0 at the base. Rather than imposing the sigmoidal transition, which was highly subject-specific, we imposed a step function instead for the purposes of this study. P_{LVendo} and P_{RVendo} were the pressures applied to the left and right endocardial surfaces, respectively, and was prescribed by two independent piece-wise functions that describe the five-phases (not including initiation) of the cardiac cycle:

- *Phase 0: Initiation.* Endocardial pressures were linearly increased to reach diastasis values P_{RVDS} and P_{LVDS}.
- *Phase 1: Active diastolic filling*. Endocardial pressures were linearly increased over time t_{EDP} to end diastolic values EDP_{LV} and EDP_{RV} to mimic the effect of atrial contraction.
- *Phase 2: Isovolumetric contraction*. Electrical activation ensues and active contraction develops. During this, the ventricular pressure was controlled such that the volume was maintained to be constant via:

$$dP_{\mathrm{LVendo}} = \frac{-1}{C_{P_{LV}}} dV_{\mathrm{LVendo}} - \frac{1}{C_{V_{LV}}} \frac{dV_{LVendo}}{dt}$$
$$dP_{\mathrm{RVendo}} = \frac{-1}{C_{P_{RV}}} dV_{\mathrm{RVendo}} - \frac{1}{C_{V_{RV}}} \frac{dV_{RVendo}}{dt}$$

Where $C_{pLV}, C_{pRV}, C_{VLV}, C_{VRV}$, were the inverse of penalty terms for volume difference and volume rates for the left and right ventricles, respectively. The volume rate term was used as stabilisation against spurious oscillations of the ventricular pressure, which might occur due to inertial effects.

- *Phase 3: Ejection.* When the ventricular pressure surpasses the aortic P_{AO} and pulmonary artery P_{PA} pressures, the ejection phase begins. To model the blood pressure of the systemic circulation system during the ejection phase, the following two element Windkessel model was used:

$$C_{AO}\frac{dP_{AO}}{dt} + \frac{P_{AO}}{R_{AO}} = \frac{-dV_{\mathrm{LVendo}}}{dt}$$
$$C_{PA}\frac{dP_{PA}}{dt} + \frac{P_{PA}}{R_{PA}} = \frac{-dV_{RVendo}}{dt}$$

Where C_{AO} and C_{PA} were the compliance of the aortic and pulmonary arteries, respectively, and R_{AO} and R_{PA} were the resistance of the aortic and pulmonary circuits, respectively. During the ejection phase, the ventricular pressures P_{LVendo} and P_{RVendo} were modelled as equal to the arterial pressures P_{AO} and P_{PA} respectively, disregarding negligible pressure gradients across the arterial valves.

- *Phase 4: Isovolumetric relaxation*. This phase was triggered when the ventricular flow reverses $\dot{V}_{LVendo} > 0$, and $\dot{V}_{RVendo} > 0$, and it follows the same formulation as the isovolumetric contraction Phase 2.
- *Phase 5: Passive filling*. This phase begins when the endocardial pressure drops below the left and right atrial pressures P_LA, P_RA. The pressure was prescribed so that the two ventricular volumes were returned to its diastasis value (DSV_LV, DSV_RV).

$$dP_{\mathrm{LVendo}} = \frac{-1}{C_{pLAV}}(V_{LVendo} - DSV_{LV}) - \frac{1}{C_{vLAV}}\frac{dV_{LVendo}}{dt},$$
$$dP_{\mathrm{RVendo}} = \frac{-1}{C_{pRAV}}(V_{RVendo} - DSV_{RV}) - \frac{1}{C_{vRAV}}\frac{dV_{LVendo}}{dt}$$

Where C_{pLAV}, C_{pRAV}, C_{vLAV}, C_{vRAV} were the inverse of penalty terms for volume difference to DSVs and volume rates, for the left and right ventricles, respectively.

The two ventricular volumes V_{LVendo} and V_{RVendo} were calculated and updated throughout the cardiac cycle by using the divergence theorem and the assumption that the volume was constrained by a flat lid located on the aortic and pulmonary valvular planes, for right and left ventricles respectively, leading to:

$$V_{\mathrm{LVendo}} = \int_{\partial\Omega_{0_{\mathrm{LVendo}}}} J\,(x \cdot e_{AO})\left(e_{AO} \cdot F^{-T} n_0\right) d\partial\Omega_0,$$
$$V_{\mathrm{RVendo}} = \int_{\partial\Omega_{0_{\mathrm{RVendo}}}} J\,(x \cdot e_{PA})\left(e_{PA} \cdot F^{-T} n_0\right) d\partial\Omega_0,$$

Where e_{AO} and e_{PA} were defined so that $e_{AO} \cdot n_0 = 0$ on the aortic valve plane, and $e_{PA} \cdot n_0 = 0$ on the pulmonary valve plane.

Electromechanical coupling

Electrophysiological activation begins at Phase 2 of the cardiac cycle and drives the active tension generation. This is modelled at the cellular level by coupling of the Land active force generation[24] with intracellular calcium dynamics from the human cellular electrophysiology ToRORd model[23], henceforth referred to as the human cellular electromechanical ToRORd-Land model. In order to couple the ToRORd to the Land model, the Hill coefficient of calcium cooperativity and tropomyosin rate constant of the Land model were re-fitted in a previous study[26] so that physiological active tension could be produced in response to the calcium transient dynamics of the ToRORd model, which were different to the calcium transient to which the original Land model was fitted.

In the Land model, active force generation is modelled using four cross-bridge cycling states (blocked, unbound, pre-power stroke and the force-generating state) and the transition rates between each were calibrated to human skinned myocyte data[24]. The ToRORd-Land coupling is bidirectional, where calcium from the ToRORd binds to troponin C and drives the transition between the blocked and unbound states of the crossbridge system, while the binding of calcium from the Land model acts as a buffer for the ToRORd calcium transient. Furthermore, the length-dependence of troponin calcium affinity/sensitivity in the Land model means that calcium buffering in the ToRORd is dynamically affected by tissue deformation. The Land model was first constructed using skinned myocyte data, then several of the parameters were re-fitted to enable sufficient ejection at the ventricular scale, including the transition rate from the pre-power stroke to force-generating state of the cross bridge (k_{ws}), the sensitivity of troponin to calcium binding (Cal50)[24]. At the tissue level, the active tension was then added to the stress tensor to drive mechanical contraction[10].

Literature-informed parameter initialisation

Model parameters were initialised as listed in Table 1. Ionic time constants and conductance values were set to baseline values of the human membrane kinetics ToR_ORd model, which had been calibrated to patch clamp, action potential and calcium transient data[23]. The active tension Land model parameters were as previous calibrated to achieve a physiological calcium transient[26]. The sensitivity analysis ranges in Table 1 were determined following the assessment strategy described above.

Verification of numerical solver

Mechanical verification has been treated in more detail in a previous publication[10]. Here, we adopt a set of benchmark problems proposed by Land et al. to verify that the mechanical solver scheme is free from volumetric locking effects. Specifically, we implemented the passive inflation and compared the simulated displacements with the results of simulation across multiple different cardiac mechanics solvers to provide evidence of numerical verification. Details of these benchmarks can be found in the original paper and are briefly explained in Appendix 1. The reader is referred to previous studies for mesh convergence analyses[56] and sensitivity analyses in an idealized ellipsoid geometry[10].

Calibration to ECG and pressure-volume biomarkers

The 12-lead ECG signals of a female healthy volunteer with similar myocardial mass (108 g) as the biventricular mesh (96 g) was extracted and beat-averaged[33] for calibration of electrophysiological activation and repolarisation characteristics. The conduction velocities along the fibre and sheet-normal directions were extracted from surgical measurements[57]. The root nodes of earliest activation on the endocardial surface as well as the conduction velocities on the endocardial surface and transmurally were calibrated using the QRS segment of the ECG signal, while spatial heterogeneity in the slow rectifier potassium current (IKs) was calibrated to the ST-T segment of the ECG signal, using a Bayesian-based inference method[18,33]. The calibrated model had a transmural conduction velocity of 48 cm/s, and the fibre and sheet-normal conduction velocities were set to 67 cm/s and 44 cm/s as measured using plunge needle in control subjects[57], and the Purkinje fibres conduction velocity was set to 300 cm/s[58]. The diffusivity model parameters were tuned to achieve the specified myocardial conduction velocities at the mesh resolution used in simulations.

When the initialised parameter values were used in a preliminary electromechanical simulation, the results undershot healthy values of left ventricular peak systolic pressure by 2 kPa, ejection fraction by 32%, stroke volume by 29 mL, and peak ejection rate by 142 mL/ms, and peak filling rate by 207 mL/ms, and overshot the end systolic volume by 18 mL, and the peak pressure upstroke velocity by 70 kPa/ms. This demonstrated the need for model calibration and explorations of model uncertainties.

Due to the high computational cost of ventricular electromechanics simulations, calibration methods that require high volume of evaluations were infeasible. In this study, we designed a sequential calibration strategy based on knowledge of model sensitivities (described in detail in Appendix 1), targeting multiple quantities of interest in order of clinical important: LVEF, peak systolic pressure, peak ejection rate, and peak filling rate. This involves a series of sampling and parameter selections as follows, where single parameters were uniformly sampled and multiple parameters were sampled using Latin Hypercube Sampling:

1. Sample ejection pressure threshold, Kct, Cal50 and k_{ws} jointly and the parameter set yielding the highest LVEF was selected. These parameters were grouped together because they affect both LVEF and peak systolic pressure simultaneously, through residual active tension, cross-bridge cycling rate, myocardial compressibility, and ejection onset respectively, making independent tuning of each unfeasible.
2. Sample arterial resistance R_{LV} to match peak systolic pressure, since peak systolic pressure is directly dependent on arterial resistance in the Windkessel model.
3. Sample GCaL to further increase LVEF, which consistently undershot the physiology target following Step 2. Even a two-fold increase in GCaL remains within the physiological variability bounds applied in previous studies, and the resulting action potential duration was verified to remain within physiological ranges.
4. Sample k_{ws} again to match peak ejection rate and dP/dt_{max} while maintaining LVEF within target range. k_{ws} is the dominant parameter affecting peak ejection rate and dP/dt_{max} in the sensitivity analysis, and resampling at this stage allows fine-tuning of ejection dynamics without substantially compromising the LVEF achieve in previous steps.
5. Sample diastolic volume change parameter C_{pLAV} to match peak filling rate.

Validation by comparison to deformation and strain biomarkers

The calibrated model was evaluated against displacement and strain biomarkers as listed in Table 2 and not used for model calibration. Atrioventricular plane displacement was calculated by tracking the longitudinal displacement of the top 10% of the geometry using the apex-to-base ventricular coordinate. Wall thickness was calculated using perpendicular projections of the endocardial and epicardial surfaces. Myocardial strains were evaluated at a mid-ventricular short axis slice and at a four-chamber longitudinal, to match DENSE measurements.

Circumferential, radial, and fibre strains were evaluated using the short axis slice, while the longitudinal strain was evaluated using the long axis slice. The strain transients were then time-shifted to begin at the end of diastolic filling (Phase 1) and offset by the end diastolic strain, to match DENSE measurements.

Sensitivity analysis at cellular and ventricular scales

A global sensitivity analysis was first performed at the cellular scale using the human cellular electromechanical ToR_ORd-Land model[26] to identify the key parameters that affect active tension and action potential duration. The conductances of all ionic currents as well as troponin calcium sensitivity and the cross-bridge power stroke rate and myosin head attachment rates (k_{ws} and k_{uw}) were varied from 50% to 200%. The key parameters that affect active tension dynamics and action potential duration were identified through ranking the parameters using the total Sobol index. This analysis showed that the key parameters which affected active tension amplitude, duration, and upstroke were GCaL, SERCA, calcium sensitivity Cal50, the cross-bridge cycling rate (k_{ws}) and GNaL (Appendix Figure 1).

At the ventricular scale, the mechanical and haemodynamic parameters listed in the final column of Table 1 along with the cellular parameters GCaL, SERCA, Cal50, kws, and GNaL were included one-at-a-time sensitivity analyses, varying each parameter uniformly in a total of eight simulations each over the ranges as specified in Table 1 for mechanical and haemodynamic parameters and over 50% and 200% for cellular parameters. Each biomarker as listed in Table 2 were evaluated, and linear regression was performed.

Parameter-biomarker relationships that had p-values less than 0.05 and absolute r-values larger than 0.6 were considered significant and linear relationships. The magnitudes of biomarker effects were normalised by the maximum magnitude for each biomarker. To visualise the relative importance of model parameter on simulated biomarker, a summary diagram was generated with lines linking each parameter to each biomarker. The colour of each line indicated a positive (red) or a negative (blue) relationship. The thickness of each line was scaled by the normalised magnitude of the effect. The transparency of each line was scaled by the r-value as measure of the linearity of relationship (Results Figure 3).

Computations and software

Cellular electrophysiological simulations and Latin Hypercube Sampling were performed using bespoke MATLAB codes. Coupled cellular electromechanics, as well as biventricular electromechanics simulations, were performed using the high-performance numerical software, Alya for complex coupled multi-physics and multi-scale problems[56] on the JURECA pre-exascale module supercomputer operated by Juelich Supercomputing Centre, Germany, through a PRACE-ICEI (project, as well as on the ARCHER2 supercomputer provided by the UK National Supercomputing Service through the CompBioMedX project (Computational Biomedicine a the Exascale) funded by EPSRC under grant agreement EP/X019446/1. Code for the generation of simulation files for multi-scale sensitivity analysis, calibration and validation, as well as scripts for evaluation of ECG, PV, deformation and strain biomarkers from ventricular simulations can be found at: *https://github.com/jennyhelyanwe/Alya_input_setup/*

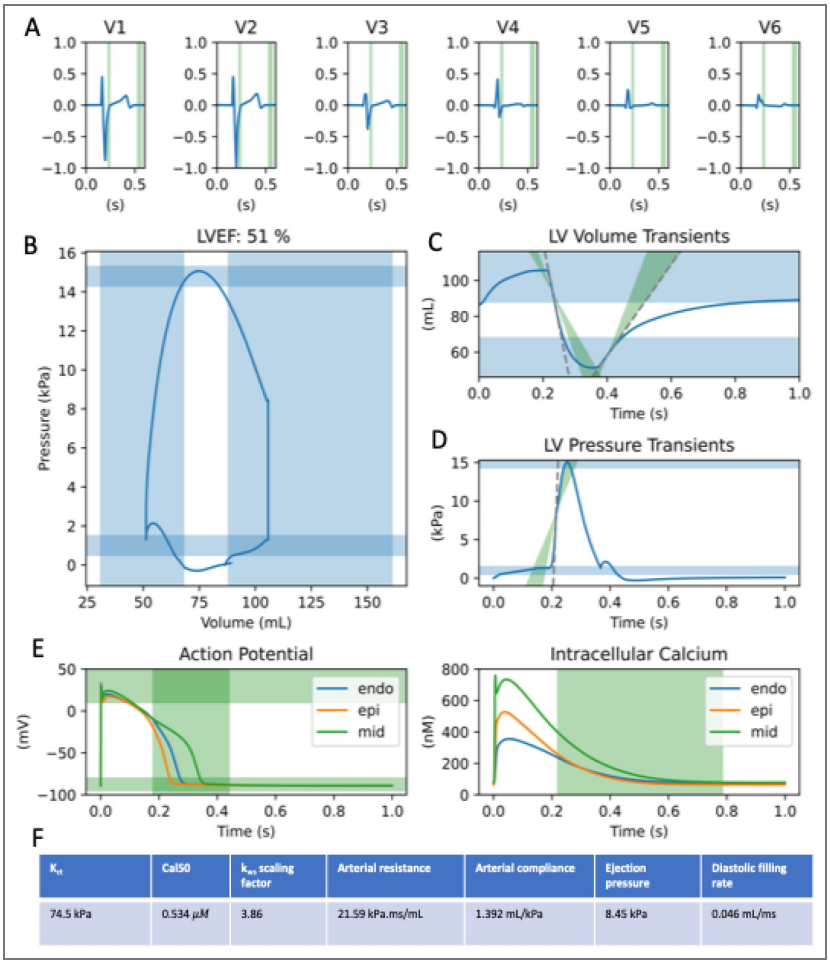

Figure 1.

Comparison of (A) simulated ECG, (B) pressure-volume, (C) flow rate, (D) pressure upstroke, and (E) cellular action potential and calcium transient biomarkers of the calibrated baseline electromechanical model with healthy population data ranges shown in green, except for (B, C, D) where the pressure volume ranges were shown in blue. The calibrated model parameters were show in the table (F).

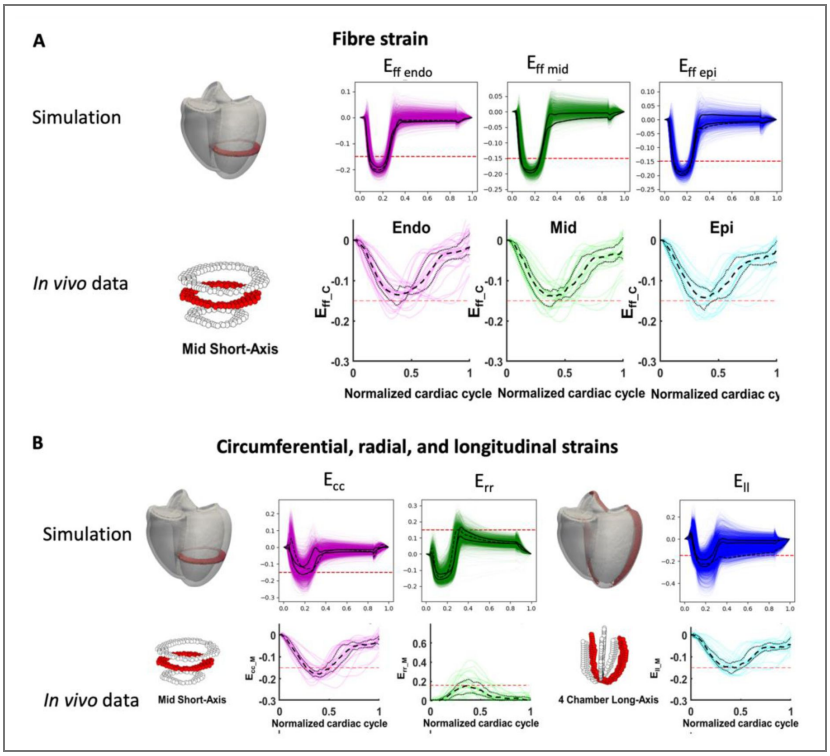

Figure 2. Comparison of simulated baseline left ventricular strains with non-invasive DENSE+cDTI MRI (in vivo) measurements.

(A) Comparison of strain along the myofiber direction measured in the mid-short-axis of the ventricles. (B) Comparison of strains in the circumferential and radial directions measured in a mid-short-axis slice and longitudinal strains measured in a four-chamber long axis slice. Median trace is plotted in dotted lines, while upper and lower quartiles in solid lines.

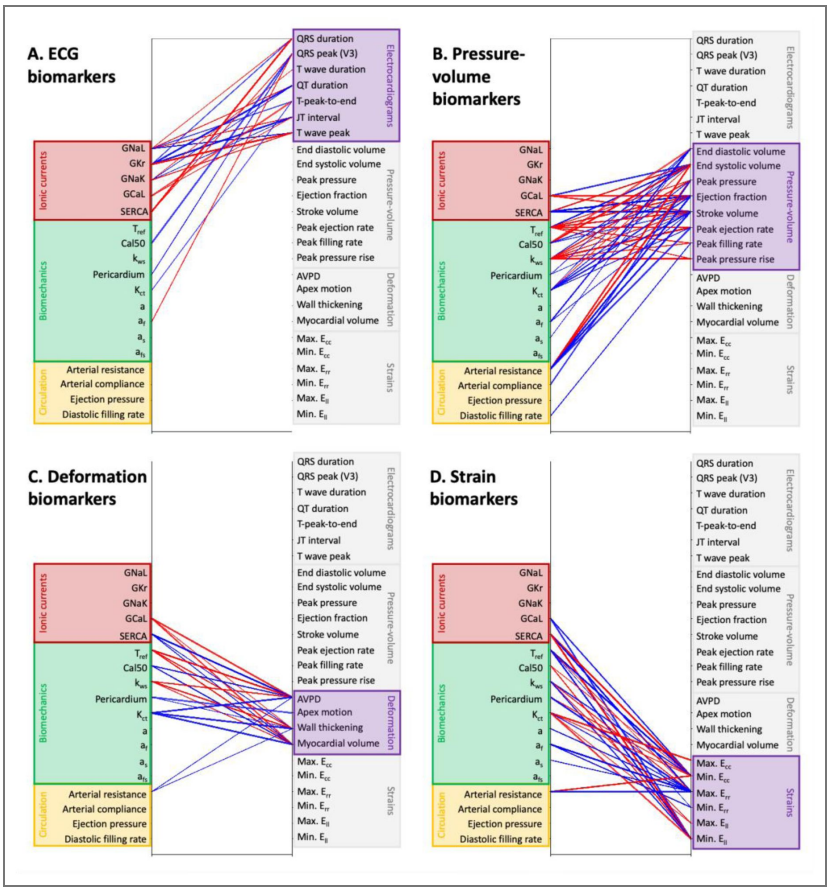

Figure 3. The effect of variability in single model parameters in cellular ionic conductances (red), passive and active biomechanical parameters (green), and circulatory model parameters (yellow) on simulated biomarkers of the ECG (A), pressure-volume (B), deformations (C), and strains (D).

Only relationships with p-value <0.05 and r-values higher than 0.6 were plotted. Positive correlations are shown in red, and negative correlations shown in blue. The thickness of each line indicates the normalised magnitude of effect and the width of each line indicates the r-value of the relationship.

Results

Experimental and clinical dataset for model calibration and validation

Table 2 presents the experimental and clinical dataset for calibration of healthy human ventricular electromechanics. For pressure-volume biomarkers and ECG biomarkers, reported values from the UK Biobank[1] were used, where the number of samples reaches the tens of thousands. Catheter measurements of intraventricular pressure dynamics were rare in the literature and have small dataset sizes.

Model verification

The simulations of the passive inflation problem set out in the Land (2015) benchmark paper[82] matched well the observed displacements across different cardiac mechanics solvers (Figure A1). Electrophysiological verification of mesh resolution sufficiency was supported by tuning diffusivity parameters to achieve the specified myocardial conduction velocities, following a previous approach[33], using an Alya-specific implementation of tuneCV (*https://github.com/rsachetto/MonoAlg3D_C/tree/master/scripts/tuneCV*).

Biventricular electromechanics model calibration to ECG and pressure-volume biomarkers

Following model calibration, the simulated ECG showed good R wave progression from V1 to V6 and QRS duration that fell within the ranges shown in Table 1 (Figure 1A) as well as simulated left ventricular ejection fraction of 51% and peak systolic pressure of 14 kPa, with end diastolic and end systolic volumes of 110 mL and 50 mL (Figure 1B, C, D), and a peak filling rate of 310 mL/ms (Figure 1D), all falling within 95% interval of physiological biomarker ranges as listed in Table 1. At the cellular scale, action potential duration, resting membrane potential, peak potential, intracellular calcium transient duration of the calibrated were all within physiological ranges (Figure 1E). The right ventricular end diastolic and end systolic volumes also fell within physiological ranges, though the right ventricular ejection fraction and peak pressure did not, as this was not a key target for calibration. The calibrated model overshot the peak pressure upstroke by 30 kPa/ms and peak ejection rate by 180 mL/ms (Figure 1D). However, the importance of matching to these two biomarkers is lower compared with other haemodynamic markers due to the relative paucity of reported data: n=17 for peak pressure upstroke and n=15 for peak ejection rate, compared with n=804 for ejection fraction and n=150 for peak systolic pressure (Table 2), It is also possible that the calibration could be improved by including some additional model parameters, such as those relating to stretch-rate dependent force generation, even though they did not show a strong effect on single cell active tension upstroke (Appendix Figure A1). These additional parameters might have a stronger effect on the upstroke at ventricular scale than at single cell scale because the single cell simulations were performed under isometric conditions. The calibrated model parameters are listed in Figure 1F.

Validation by comparison to deformation and strain biomarkers, not used in calibration

Table 3 presents the experimental and clinical dataset for validation of calibrated healthy human ventricular electromechanics. Mechanical displacement and strain biomarkers came from MRI studies with specialised sequences (e.g. DENSE strain imaging).

Simulation showed broad agreement with the trend and magnitude of *in vivo* strain measurements from DENSE+cDTI images[55] for fibre strain, circumferential, radial, and longitudinal strain in mid-ventricular and four-chamber view slices (Figure 2, Table 3). Simulated strain traces (n=5004 for short axis, n=9282 for long axis) showed higher variability than *in vivo* traces (n=30). Simulated fibre strain (Eff, Figure 2A) showed agreement in terms of

Validation dataset				
Biomarker	**Simulated**	**Reference Ranges**	**Data info**	**Implication for cardiac diseases**
ED wall thickness (cm)	0.5	[0.57, 1.38]$_{range}$ [83]	mixed sex, range of mean values over 17 AHA regions, UKBB CMR, n=4620	Increased in HCM or HHD[84,85]
ES wall thickness (cm)	0.7	[1.07, 1.749]$_{range}$ [83]	mixed sex, range of mean values of 17 AHA regions, UKBB CMR, n=4620	Fractional thickening reduced in HCM[85]
Atrioventricular plane displacement (AVPD) (ES – ED) (cm)	1.5	[1.4, 1.9]$_{range}$ [54]	mixed sex, CMR, healthy subjects n=12	Reduced in DCM[54]
Systolic global longitudinal strain (Ell)	-0.23	−0.16 [−0.16, −0.16]$_{IQR}$ [55]	four chamber slice, mixed sex, cDTI + DENSE, n=30	Major predictor of LV dysfunction and HF, greater accuracy than LVEF[86,87]
Systolic radial strain (Err)	0.15	0.27 [0.22, 0.29]$_{IQR}$ [55]	Short axis slices, mixed sex, cDTI + DENSE, n=30	Associated with chronic HF[88]
Systolic circumferential strain (Ecc)	-0.15	-0.10 [-0.14, -0.08]$_{IQR}$ [55]	Short axis slices, mixed sex, cDTI + DENSE, n=30	Associated with chronic HF[88]

Table 3. Comparison of simulated validation outputs against reference ranges for deformation and strain biomarkers not used in model calibration.

Reference ranges are as reported in Table 2. AVPD: atrioventricular plane displacement, E_ff: fibre strain, E_cc: circumferential strain, E_rr: radial strain, E_ll: longitudinal strain.

transmural homogeneity when compared with *in vivo* measurements, and the magnitude of fibre shortening was similar to *in vivo* (compare with red line at -0.15 strain). Quantitatively, the simulated average peak strains were E_{ff}=-0.20, E_cc=-0.15, E_rr=0.15, and E_ll=-0.23, which fall within or close to the reference ranges reported in Table 2 and showed good agreement in magnitude with *in vivo* measurements (compare with red lines in Figure 2). Radial strain was underestimated relative to the reference range, which is derived from a cohort of 30 subjects and therefore represents a relatively narrow population sample. The timing of simulated peak strains occurred earlier than that *in vivo*. However, this is partially because the model was not calibrated to the cardiac cycle timings of the single individual in the DENSE+cDTI dataset.

In terms of deformations, the simulated systolic vs diastolic atrioventricular plane displacement of the calibrated biventricular (1.5 cm) showed good agreement with ranges reported in the literature (1.4 to 1.9 cm, Table 3). When compared with literature reports of wall thickness changes, simulations showed thickening in systole in agreement with literature. The simulated end diastolic wall thickness (0.5 cm) was lower than the report range [0.57, 1.38] cm (Table 3), and the end systolic wall thickness (0.7 cm) was also lower than the report range of [1.07, 1.75] cm (Table 3). The low wall thickness in both diastole and systole were consistent with the small heart size of the example used (96 g ventricular mass), and a larger and thicker heart would have greater wall thickening and fall better within the population ranges.

One-at-a-time sensitivity analysis

Figure 3 summarises how variability in single model parameters relate to simulated ECG (Figure 3A), pressure-volume (Figure 3B), displacement (Figure 3C), and strain (Figure 3D) biomarkers. Positive relationships between parameter and biomarker were shown in red and the negative were shown in blue.

ECG biomarkers (Figure 3A) were mostly affected by variabilities in ionic conductances (red block), with some small effects from the mechanical parameters (green block). QRS effects were very minimal, since conduction velocities were not altered in the analysis. QRS duration altered by SERCA (magnitude of change: 2.8 ms), GCaL (1 ms), GKr (1.8 ms), and GNaL (1.3 ms), while normalised QRS amplitude in lead V3 was very weakly affected by calcium sensitivity Cal50 (magnitude of change: 0.04), pericardial stiffness k_{epi} (0.01), and the passive stiffness parameter a_f (0.02) (Appendix Figure A1.A). The ST and T wave segments were much more sensitive to model parameters. The QT interval was strongly affected by GKr (magnitude of change: 173 ms), GNaL (92 ms), GNaK (72 ms), GCaL (69 ms), and SERCA (49 ms), with weak effects from calcium sensitivity (Cal50) (1.7 ms). Normalised T wave amplitude was affected by GKr (magnitude of change: 0.1), GNaK (0.06), GNaL (0.06), and SERCA (0.04), GCaL (0.03), with very minor (<0.01) amplitude changes in select precordial leads for Tref (lead V4), Cal50 (lead V4), pericardial stiffness (lead V3) and Kct (lead V2) (Appendix Figure A1.B).

Pressure volume biomarkers (Figure 3B) were mostly affected by the mechanical (green block) and circulatory parameters (yellow block), alongside ionic currents (red block) that affect the calcium signaling system (GCaL and SERCA). Appendix Figure A2 illustrates in detail the parameter effects on the pressure-volume loops. The ejection fraction was predominantly affected by cross-bridge power-stroke rate (k_{ws}) (magnitude of change in ejection fraction: 32 %), compressibility (Kct) (16 %), GCaL (15 %), peak active tension (Tref) (12 %), SERCA activity (10 %). There were also some effects on LVEF from GNaL (9%), arterial resistance (6 %), calcium sensitivity (Cal50) (8 %), and very weak effects from pericardial stiffness (4 %), passive mechanical parameters a (3 %), a_f (2 %), a_s (4 %), and GNaK (2 %), and GKr (2 %). Our models showed that Cal50 not only affected systolic but also diastolic function through altering the diastolic residual active tension, which could contribute to prolonged relaxation in heart failure[89].

The peak systolic pressure was affected by the same parameters as the ejection fraction, except for GNaK, GNaL and GKr, and with the addition of arterial compliance (magnitude change: 1.1 kPa) and ejection pressure threshold (1.9 kPa). The peak rate of rise of ventricular pressure (dPdtmax) was strongly influenced by only the cross-bridge power-stroke rate (k_{ws}) (magnitude of change: 1 kPa/s), with weak effects from calcium sensitivity (Cal50) (0.6 kPa/s) (Appendix Figure A3.A). The

peak ejection flow rate (PER) was influenced by Cal50, Tref, k_ws, while the peak filling rate (PFR) was influenced by a larger group of parameters including Tref, Cal50, Kct, GCaL, SERCA, and the bulk parameter controlling the diastolic filling rate (Appendix Figure A3.B).

Mechanical displacement biomarkers (Figure 3C) were predominantly affected by active mechanics (green block) and calcium system conductances (red block), with very minor effects from passive mechanical parameters. Systolic AVPD (Appendix Figure A4.A) was strongly influenced by Cal50 (magnitude of effect: 0.54 cm), GCaL (0.36 cm), Tref (0.33 cm), Kct (0.41 cm), SERCA (0.31 cm), with weaker effect from k_{ws} (0.15 cm), arterial resistance (0.09 cm), and pericardial stiffness (0.08 cm). Systolic wall thickness was predominantly affected by the same parameters as systolic AVPD, except for Kct, which had only a weak effect. Systolic percentage volume change (Appendix Figure A4.C) was strongly affected by the compressibility parameter (Kct) (magnitude of change: 12 %), as was expected, but also strongly affected by GCaL (9 %), Tref (8 %), SERCA (6 %), and kws (3 %). An increase in SERCA and Cal50 shifted the timing of peak volume reduction to earlier during systole.

Simulated strain biomarkers (Figure 3D) were predominantly affected by passive mechanical parameters (green block) and circulatory parameters (yellow block). The influence of parameters on the radial, circumferential and longitudinal strain patterns (Appendix Figure A5) followed broadly that of the AVPD and wall thickness. Of note was that at high values of the ejection pressure, the mid-ventricular circumference expands rather than contracts during systole and fails to return to the reference condition even after relaxation, pointing to failure of proper pumping function (Appendix Figure A5.A).

Multi-scale mechanisms underpinning ECG and LVEF relationship

Simulation results indicated that the link between ECG biomarkers and LVEF was chiefly underpinned by GCaL and SERCA, which had strong effects on both T wave biomarkers and the pressure-volume loop (Figure 3). Mechanical parameters T_{ref}, calcium sensitivity (Cal50), compressibility (Kct), and fibre stiffness (a_f) had much stronger effects on LVEF than on ECG signatures. On the other hand, ionic conductance parameters GNaL, GKr, GNaK had much stronger effects on the T wave than on LVEF.

Figure 4 illustrates the multi-scale mechanisms of GCaL's effect on both LVEF and ECG. A four-fold increase in GCaL caused an eight-fold increase in cellular active tension peak and a 200 ms prolongation of active tension duration (Figure 4A), which resulted in a 15 mL decrease in end systolic volume and 2.5 kPa higher peak systolic pressure at the ventricular scale (Figure 4C). GCaL's dramatic effect on end systolic volume was facilitated by 10 % higher systolic myocardial volume compression, 4.5 % higher systolic longitudinal contraction (Figure 4E, dotted lines), 3.5 % higher systolic circumferential contraction, and 0.4 cm lower (towards apex) systolic position of the atrioventricular plane (Figure 4B). The increase in longitudinal contraction was achieved by a greater downward motion of the basal plane while the apex stayed stationary due to the pericardial constraint. The increase in GCaL caused an increase of 60 ms in cellular action potential duration (Figure 4A), which prolonged the global repolarisation time (Figure 4D) and led to the prolongation of the QT interval (Figure 4C). GCaL did not have a significant effect on the activation pattern and conduction velocity in our simulations (Figure 4D) or on the QRS complex of the ECG (not shown).

Figure 5 illustrates how a four-fold increase in SERCA activity caused a 12% decrease in LVEF, with non-monotonic effects on the QT interval. The increase in SERCA conductance increased diastolic residual active tension (Figure 5A), which was sufficient to cause 3 mL reduction in end diastolic volume (Figure 5C). Even though increasing SERCA increased peak active tension at the cellular scale by 9 kPa (Figure 5A), it reduced peak systolic pressure and LVEF at the ventricular scale (Figure 5C). This was because increasing SERCA hastened the arrival of peak active tension by 50 ms and reduced its duration by 100 ms (Figure 5A), which meant that the mechanical contractions were not given enough time to developed, resulting in earlier and weaker systolic contractions (Figure 5B). On the electrophysiological side, while SERCA did not elicit strong APD

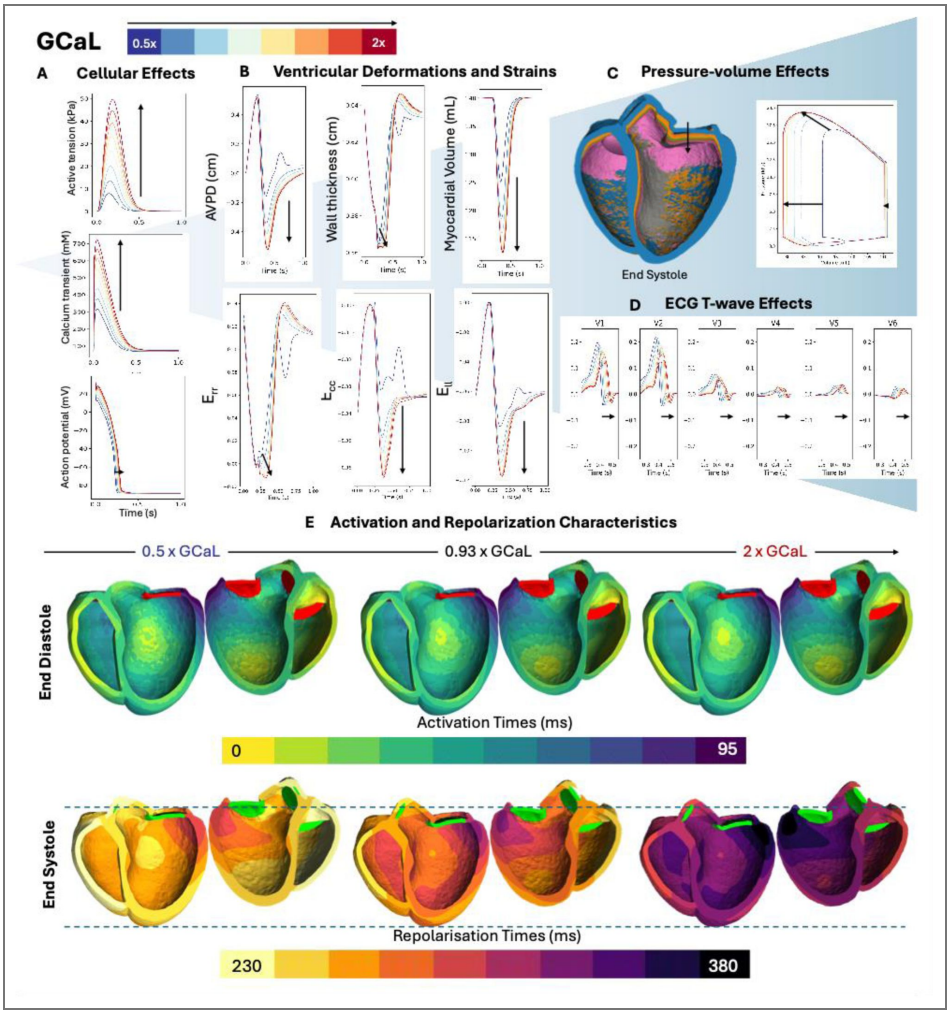

Figure 4. Multi-scale effect of GCaL on active tension, action potential duration (A), ventricular deformation and strains (B), the pressure-volume loop (C) and precordial ECG leads (D).

ECG characteristics were explained by the activation and repolarization maps (E), with dotted lines highlighting increased longitudinal shortening with increasing GCaL by the basal plane moving towards the apex while the apical position remains unchanged, due to the presence of the pericardial constraint. Scaling factor of 0.93 was the closest scaling factor to 1 when uniformly sampling eight datapoints in range [0.5, 2].

changes at the single cell simulation, when combined with non-isometric conditions in ventricular simulations, it caused action potential prolongation at values higher than 1.5-fold and resulted in prolonged repolarization (Figure 5E).

Discussion

In this study we presented the calibration, validation and sensitivity analysis of human healthy ventricular electromechanical modelling and simulation, following the ASME V&V40-based assessment guidelines. The first step was compiling parameters and biomarkers values from multi-modal data characterizing pressure-volume, ECG, displacement, and strain behavior of human healthy ventricles, and separated the data for calibration and validation as well as identify model parameter ranges for sensitivity analysis. The calibration was informed by unravelling the interlinking relationships between simulated biomarkers and model parameters, especially highlighting the plethora of model parameters that affect the ejection fraction. We demonstrated multi-scale mechanistic explanations of the relationship between LVEF and ECG underpinned by variability in L-type calcium channel conductance and SERCA activity. Through considering biomarkers at multiple scales and across both electrophysiology and mechanics, we aimed to provide a transparent audit of current capability by identifying where confidence is established and where further development is needed, as a firm foundation for future refinement Previous examples of applying the ASME V&V40 framework for cardiac model credibility assessment have focused primarily on evaluating computational models of medical devices such as the left ventricular assist device[21] and artificial heart valves[22], where model validation was performed by comparing to experimental recordings specifically designed for this purpose. These studies, as well as other examples of model validation without explicit reference to the ASME Standard, commonly have narrow focuses on specific diseases and/or therapies, and the biomarkers used for model evaluation were similarly limited in scope. In the case of disease models, calibrations were commonly performed at the cellular or tissue scale and validation was performed at the ventricular scale through comparisons with known ECG or ejection fraction phenotypes[12,15]. While these studies have been valuable for providing model credibility in their specific disease/therapeutic contexts of use, they have not been designed to give credibility to the underlying computational electromechanics framework. In this study, we instead focused on building a comprehensive calibration and validation strategy for baseline healthy biventricular electromechanics.

We showed in this study that literature values for model parameters do not automatically provide good baseline simulations. We proposed a sequential calibration strategy based on knowledge of model sensitivities, as detailed in the methods. This approach can be adapted for more sophisticated numerical techniques involving the use of emulators and Bayesian statistics to enable faster and more comprehensive explorations of the parameter space[27,29,90], and enable matching to more stringent calibration criteria such as the inclusion of cellular biomarkers to ensure simultaneous multi-scale compliance. Non-uniform sampling of the parameters based on knowledge of parameter-biomarker relationships could also improve its efficiency.

Our sensitivity analysis results showed that in the simulated ECGs, the T wave was far more sensitive to electrophysiological parameters than to mechanical ones, within the ranges of variability expected from literature reports of each parameter. In our simulations, the ionic conductances GNaK and GNaL primarily affected the T wave through altering the action potential duration (Appendix Figure A1) while having minimal effect on mechanical deformation or strain. GCaL and SERCA strongly affected the repolarization pattern and deformation and strain patterns during systole (Figures 4 and 5). However, other parameters that had a strong effect on deformation and strain, such as Tref, Cal50, pericardial stiffness and Kct had only a minor effect on the T wave (Appendix Figure A2). Previous studies on this question focused on comparing either end diastolic versus end systolic geometry[11] or a static versus dynamic geometry[91] when simulating the T wave. These simulations involved a much larger perturbation in deformation than relevant to physiological situations and showed a larger effect on the T wave

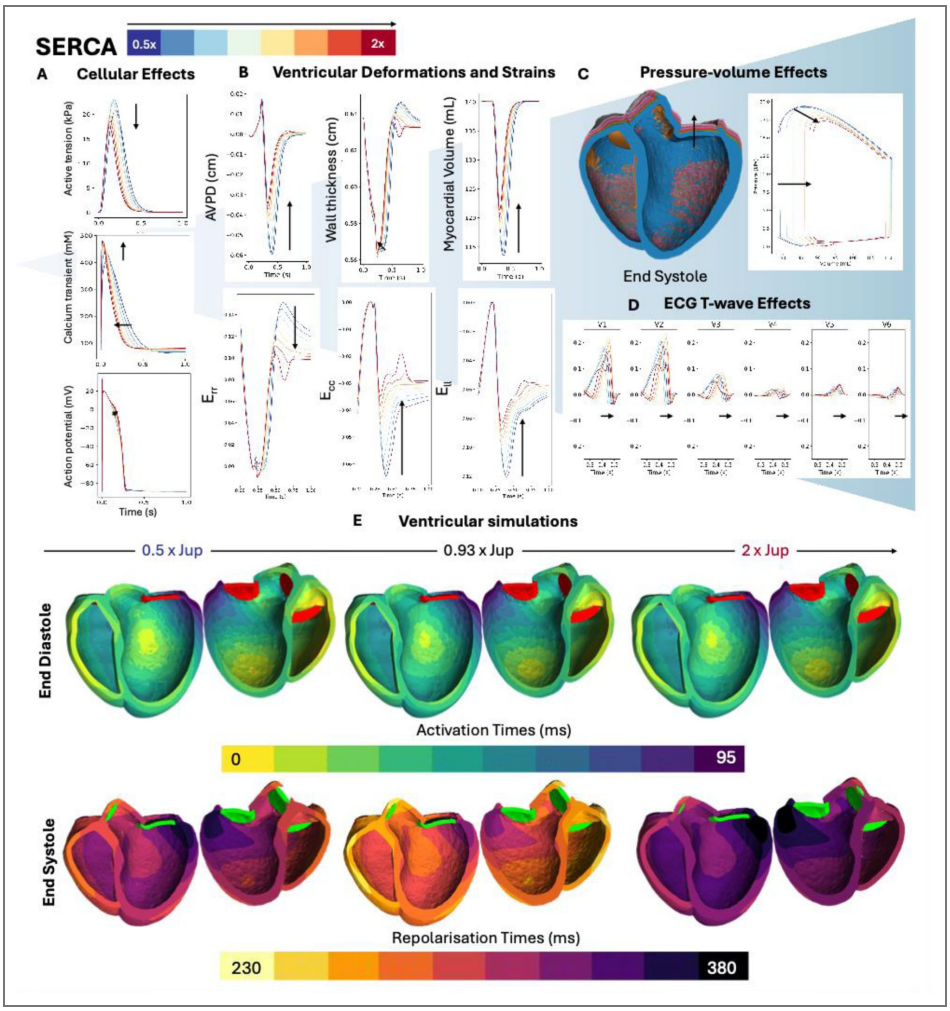

Figure 5. Multi-scale effect of SERCA conductance on active tension, calcium transient, action potential duration (A), ventricular deformation and strains (B), the pressure-volume loop (C) and precordial ECG leads (D).

ECG characteristics were explained by the activation and repolarization maps (E). Scaling factor of 0.93 was the closest scaling factor to 1 when uniformly sampling eight datapoints in range [0.5, 2].

amplitude than our simulations. Within the context of physiological systolic deformations, however, our results showed that deformation uncertainties had only minor effects on T wave amplitude.

Our simulations showed only minor changes to QRS amplitudes in response to variation in those parameters that influenced the end diastolic geometry: calcium sensitivity, through altering diastolic residual active tension, pericardial stiffness, through restricting diastolic inflation, and the passive mechanical parameters a and af, through altering bulk stiffness and stiffness along the myofibre direction. However, it is possible that the magnitude of changes to the QRS was underestimated in our simulations, because the local activation times on the endocardial surface in our simulations were fixed. This meant that our simulations did not explore the effect of variations in end diastolic geometry on the conduction velocity of the fast endocardial activation layer or on Purkinje conductivity. It should also be noted that other parameters that affect the activation pattern, such as GNa and conduction velocities, were not included in this analysis.

The fact that the initialised literature values of model parameters failed to achieve LVEF above 50 % pointed to potential limitations in our modelling approach. Our final calibrated model required a ten-fold scaling factor on the peak active tension transient, as was found to be necessary in a previous sensitivity analysis study[10]. This is a significant deviation from *ex vivo* measurements of myocardial force production, which is better understood through comparison with similar studies in the field. Strocchi et al. (2023)[32] used a four-chamber model and required a considerably more modest adjustment of active tension, likely reflecting differences in model geometry, pericardial constraint, and circulatory model.

Gerach et al. (2021) [9] achieved stroke volumes close to MRI data but report that systolic pressures in. both ventricles were too high for a healthy heart, attributing this to the steep increase in stress due to their tension model, and similarly report elevated peak ejection rates compared to MRI measurements. They also report that atrial contraction contributes a significant fraction of end-diastolic volume, a contribution absent from biventricular-only models such as ours and a primary likely factor in the compensating active tension required. Zingaro et al. (2024)[92] found that no single contractility parameter configuration simultaneously achieved physiological peak ejection rate and LVEF, consistent with our own experience. Together these comparisons suggest that the absence of atrial mechanics is a key contributor to the elevated active tension scaling in our model.

Furthermore, this could be explained by other model limitations, including volumetric locking effects, even though benchmarking our mechanical solver as in Land (2015) [1] did not show volumetric locking effects. Further analysis is, however, warranted against a more comparable elastodynamic systems with orthotropic passive mechanics, such as presented in the recent Arostica (2025) benchmark problems[93]. Other model simplifications could also contribute to the difficulty in achieving a healthy LVEF. In our simulations, we saw that the LVEF was strongly sensitive to changes in the incompressibility of the tissue (Kct), such that an increase in compressibility of the myocardial tissue helped to increase LVEF. The systolic volume has been reported to change up to 13%[1], pointing to limitations of assumptions of incompressibility in the modelling of the myocardial tissue and ignoring poro-elastic[95] and visco-elastic effects[38]. This is further highlighted by the fact that our model did not achieve a high amount of wall thickening in validation, which meant that the high compressibility required in our model to achieve LVEF could be compensating for a lack of sufficient wall thickening, in addition to anatomical effects. Previous experimental and simulations studies have shown how wall thickening is related to sliding of sheetlets[96,97]. However, in our simulations we did not see a significant effect of the sheer stiffness parameter a_{fs} on wall thickness or LVEF. Another possible avenue of exploration would be the effect of sheet and fibre orientations on the thickening effect, as explored in a previous simulation study[97].

Displacement and strain biomarkers (Figure 2D) were far more sensitive to calcium handling dynamics, cross-bridge cycling rate, and contractility than to passive stiffness parameters, which indicates they would be better indicators of systolic rather than diastolic dysfunctions in HF. The sensitivity of strains and displacements to the pericardial stiffness parameter was unsurprising

due to the association of reduced strains in diseases affecting the pericardial sack[98]. The sensitivity of longitudinal and radial strain to the incompressibility of the myocardium (Kct) mirrors the sensitivity of the LVEF to that parameter, which was in accordance with the fact that those two strains were surrogate markers of LVEF and show better predictive power[86,87].

Limitations

While the electromechanical model presented is advanced in terms of its human-relevance and multi-scale complexity, it contains modelling simplifications that can be extended in future work to allow its application to specific areas of investigation.

The model uses an isotropic downscaling of the end diastolic biventricular anatomy to approximate the unloaded reference geometry, to achieve a physiological diastasis volume. While our simplification allowed us to match population-based volume metrics, more physically accurate methods of unloading the geometry[1,2] will be necessary if the aim is to personalise mechanical stiffness parameters[100–102] and investigate diastolic dysfunction[103,104]. Moreover, even in the unloaded state, the myocardial tissue is not without residual strains[105,106] , which can be important to take into account when inferring patient-specific diastolic function.

Our lumped parameter model of the circulatory system was sufficient for capturing the calibration haemodynamic metrics but can be expanded to provide smooth transitions between phases of the cardiac cycle and additional mechanistic details on arterial dynamics[107] to better capture the time-course of pressure boundary conditions and to preserve stroke volume balance between the two ventricles.

On the epicardium surface, we model the effect of the pericardium by prescribing a spring Robin type constraint aligned with the surface normals. This constraint, while being able to produce realistic atrioventricular plane displacement, can be extended to more accurately represent frictionless contact mechanics[108] to better replicate four chamber mechanics[31,49] and can be important in investigations of pericardial dysfunction[109].

Finally, our current calibration framework primarily targets left ventricular pressure-volume biomarkers, including volumes, ejection fraction, pressure, and the ECG. Consequently, the model is not explicitly constrained to achieve equal stroke volumes between the right and left ventricles in steady state. This is an important physiological limitation which can be overcome by methods for explicitly tuning right ventricular active tension against measured right ventricle-specific data, as demonstrated by Miller et al.[110], or a more sophisticated multistep calibration procedure that sequentially optimises circulatory dynamics, passive mechanics and active contraction for both ventricles, as demonstrated by Brown et al.[111]. Both approaches represent a natural extension of the calibration framework presented here, and incorporating independent right ventricular calibration targeting stroke volume balance is a priority for future work. We note that despite the absence of explicit RV calibration, the RV volumetric measures fell within physiological ranges, though the RV peak pressure exceeded the physiological range, consistent with the stroke volume imbalance described above.

Conclusions

In this study, we show the importance of applying vigorous VVUQ evaluations of ventricular electromechanics for achieving physiological simulations and systematically identify avenues for future work. We set the basis for a strategy for calibrating and validating high-fidelity baseline electromechanical modelling and simulation frameworks. We compiled a comprehensive list of biomarkers for evaluating healthy electromechanical function, and grouped the dataset into non-overlapping calibration and validation sets. We provide evidence of credibility through calibration to haemodynamic and ECG biomarkers and validation by comparison to strain and deformation biomarkers and sensitivity analysis.

Furthermore, through multi-scale sensitivity analysis spanning both mechanical and ECG biomarkers simultaneously, our analyses highlighted the interplay between cellular, tissue, and haemodynamic parameters on the LVEF and provided multi-scale explanations of its link with ECG

biomarkers, which is an analysis not previously performed in a fully coupled electromechanical framework. The sensitivity analysis presented here, performed over biologically informed parameter ranges, provides a foundation for future uncertainty quantification studies using probabilistic inference. Taken together, the study provides a systematic framework for credibility assessment of electromechanical cardiac models, identifies open priorities for further development, and represents a meaningful step towards the cardiac Digital Twin vision.

Data availability

The current manuscript is a computational study, so no data have been generated for this manuscript. Modelling code is available at *https://github.com/jennyhelyanwe/Cardiac-Electromechanics-Workflow*

Acknowledgements

This work was funded in whole, or in part, by the Wellcome Trust (214290/Z/18/Z). For the purpose of Open Access, the author has applied a CC BY public copyright licence to any Author Accepted Manuscript version arising from this submission.

This work was supported by a Wellcome Trust Fellowship in Basic Biomedical Sciences to B.R. (214290/Z/18/Z), the Personalised In-Silico Cardiology (PIC) project, the CompBioMed 1 and 2 Centre of Excellence in Computational Biomedicine (European Commission Horizon 2020 research and innovation programme, grant agreements No. 675451 and No. 823712), the Oxford BHF Centre of Research Excellence (RE/13/1/30181), PRACE-ICEI funding projects icp005, icp013, icp019.

The authors would like to acknowledge Dr Alberto Zingaro and Dr Dimitrios Lialos from ELEM Biotech, who assisted with Alya benchmarking simulations for verification in the revised version of the manuscript.

Appendix

1. Model verification

Following the Land[93] benchmarks, we generated an ellipsoid geometry and applied pressure and Dirichlet boundary conditions as described in the benchmark. Our simulated results showed good agreement with the mean deformation reported in the original benchmark paper, verifying that the passive mechanical simulations using Alya were free from volumetric locking issues at mesh resolution of ## mm.

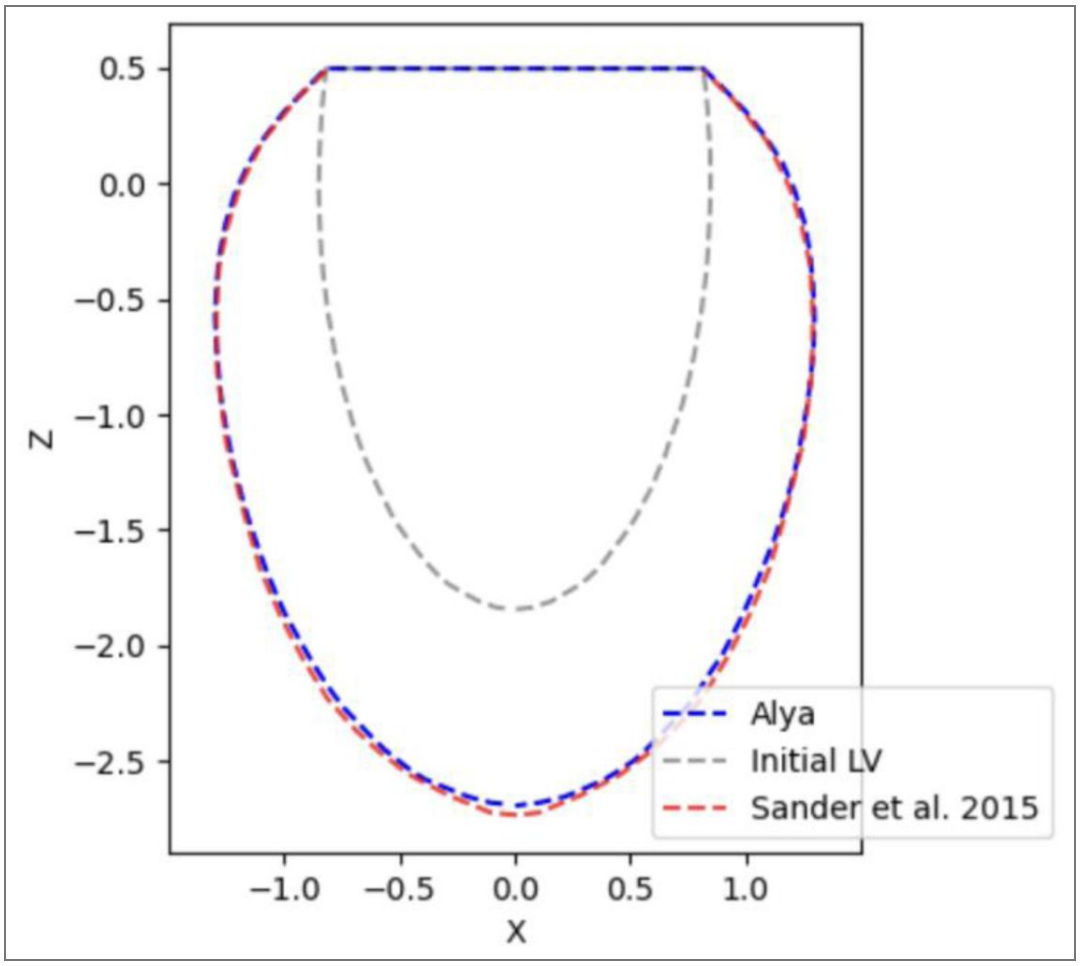

Figure A1. **Comparison of mid-line between Alya simulation (grey reference, blue deformed) and Sander Land et al. 2015 (red) passive inflation.**

Pressure volume calibration strategy design

The goal of the calibration of the initialised set of parameters was to increase LVEF, increase systolic pressure, increase peak filling rate, but decrease peak ejection rate and lower dP/dt_{max}. The LVEF and peak systolic pressure had the highest degree of importance for calibration, since they were implicated in a variety of diseases and was well established. The filling rates and $dPdt_{max}$ took a secondary role, since the data came from much smaller sample sizes, and the filling rates were measured using echocardiography techniques, which were not as reliable as volume measurements in CMR (Table 1).

From the sensitivity analysis, we saw that a handful of parameters can increase both LVEF and peak systolic pressure simultaneously: Tref, k_{ws}, GCaL, SERCA, Cal50, Kct (Figure 3). However, Tref and kws effects saturate at high values, large changes in SERCA and GCaL can become arrhythmic substrates, Cal50 has a non-monotonic effect on LVEF due to its effect on the diastolic function, and dramatic reductions in Kct brings unrealistic amounts of systolic volume change. A combination of changes in these parameters was needed to dramatically improve LVEF and peak systolic pressure, and in practice, was insufficient by themselves. Decreasing arterial resistance was also needed to help increase LVEF. However, this comes at the cost of reducing peak systolic pressure, which needed to be counterbalanced by increasing the ejection pressure threshold. An increase in ejection pressure increased time spent in isovolumic contraction and isometric force development, and thereby increased the peak systolic pressure. An additional challenge was that there was not a single parameter in our analysis that could decrease peak ejection flow rate (Tref,

kws, Kct) and $dPdt_{max}$ (kws) without also decreasing LVEF at the same time. This meant that we needed to achieve higher than healthy LVEF first. With all this in mind, the calibration strategy was as detailed in the Methods section.

2. Cellular global sensitivity analysis

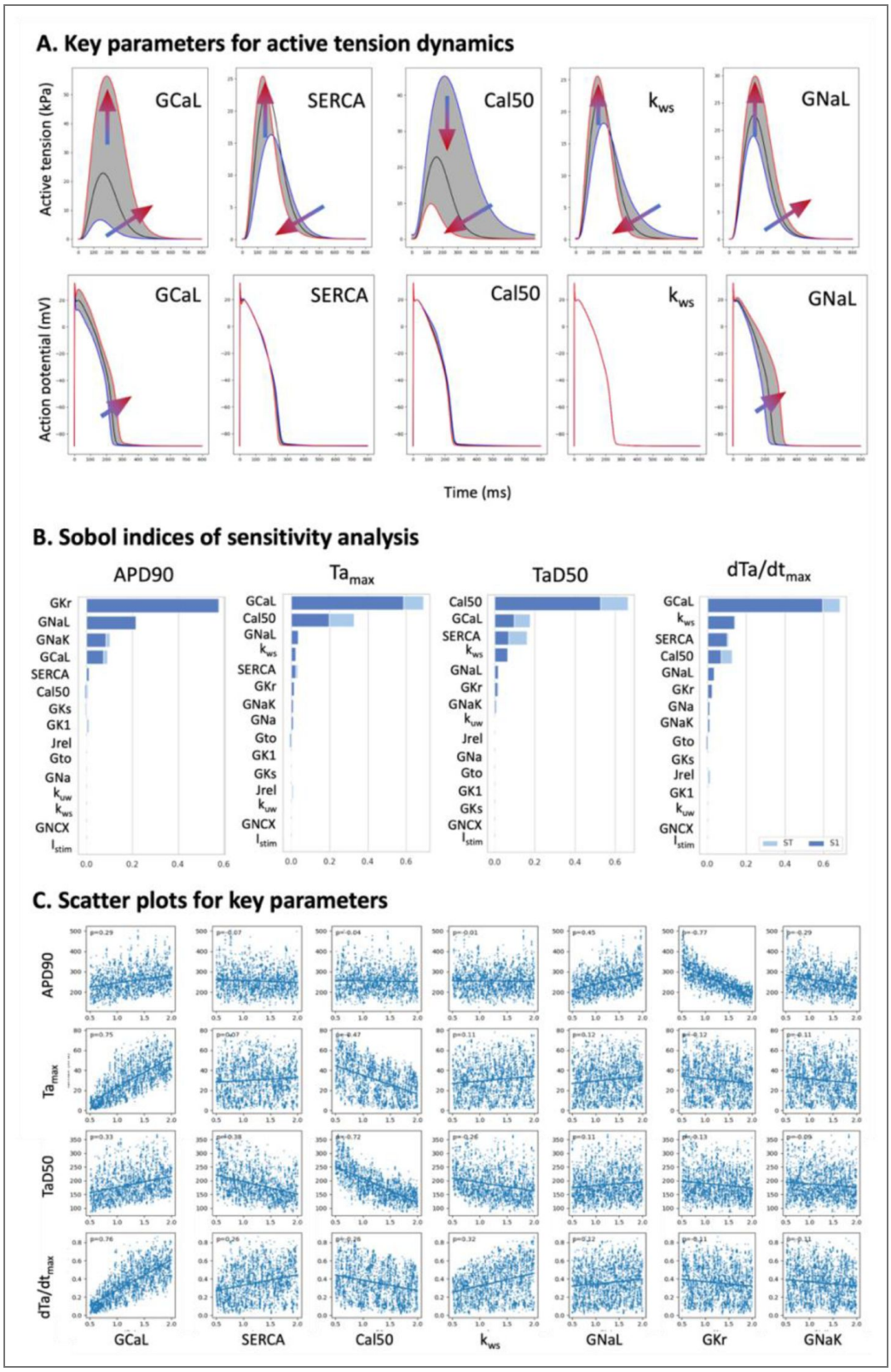

Figure A1. Global sensitivity analysis (C) using cellular model of ventricular electromechanics show the effect of the top five model parameters on active tension (A) and action potential duration (A and B) biomarkers.

3. Additional ventricular sensitivity analysis results

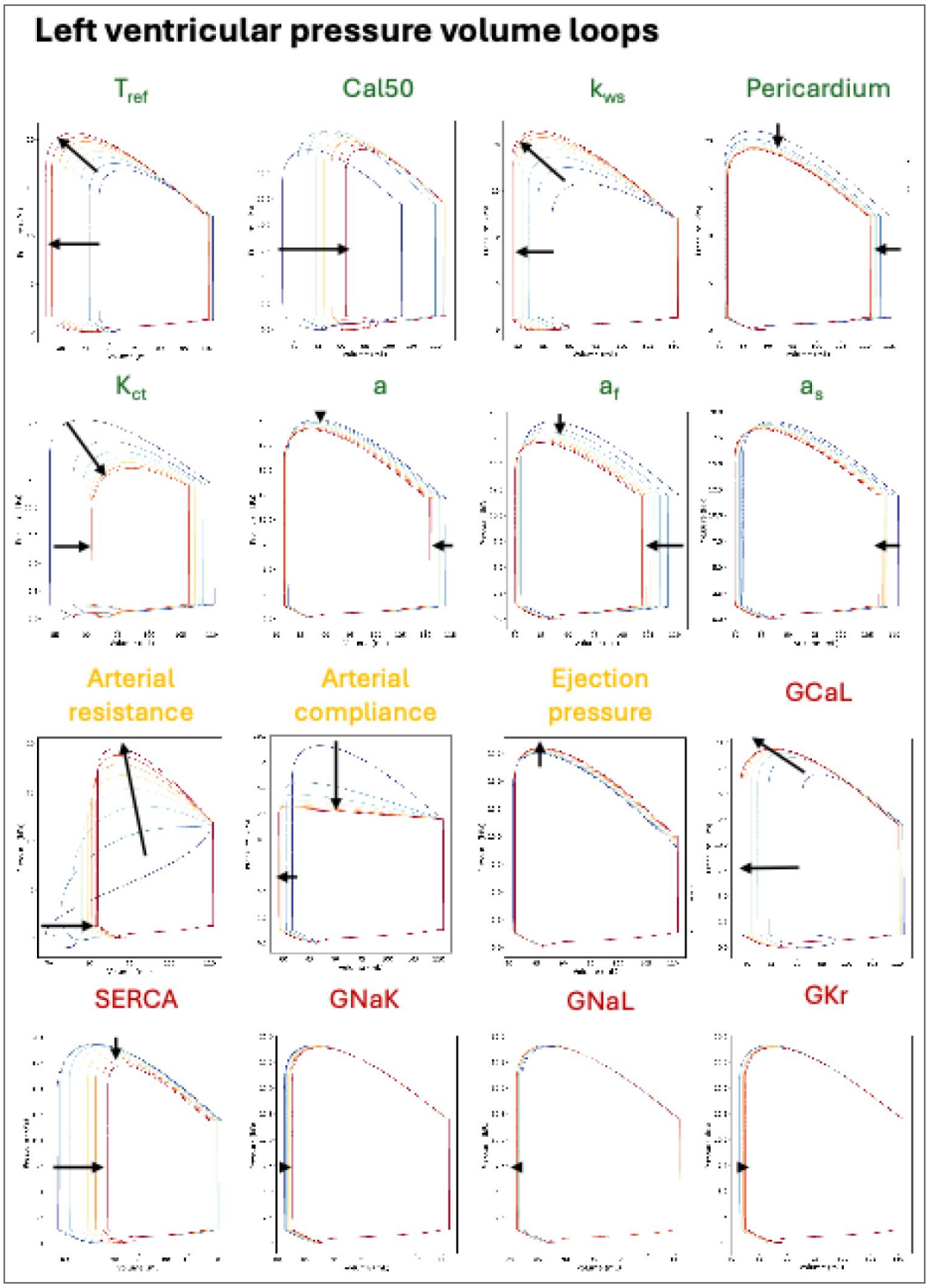

Figure A2. **Uncertainties in simulated pressure volume dynamics were influenced by uncertainties in mechanical (green), circulatory (yellow) and ionic conductance (red) parameters of the model.**

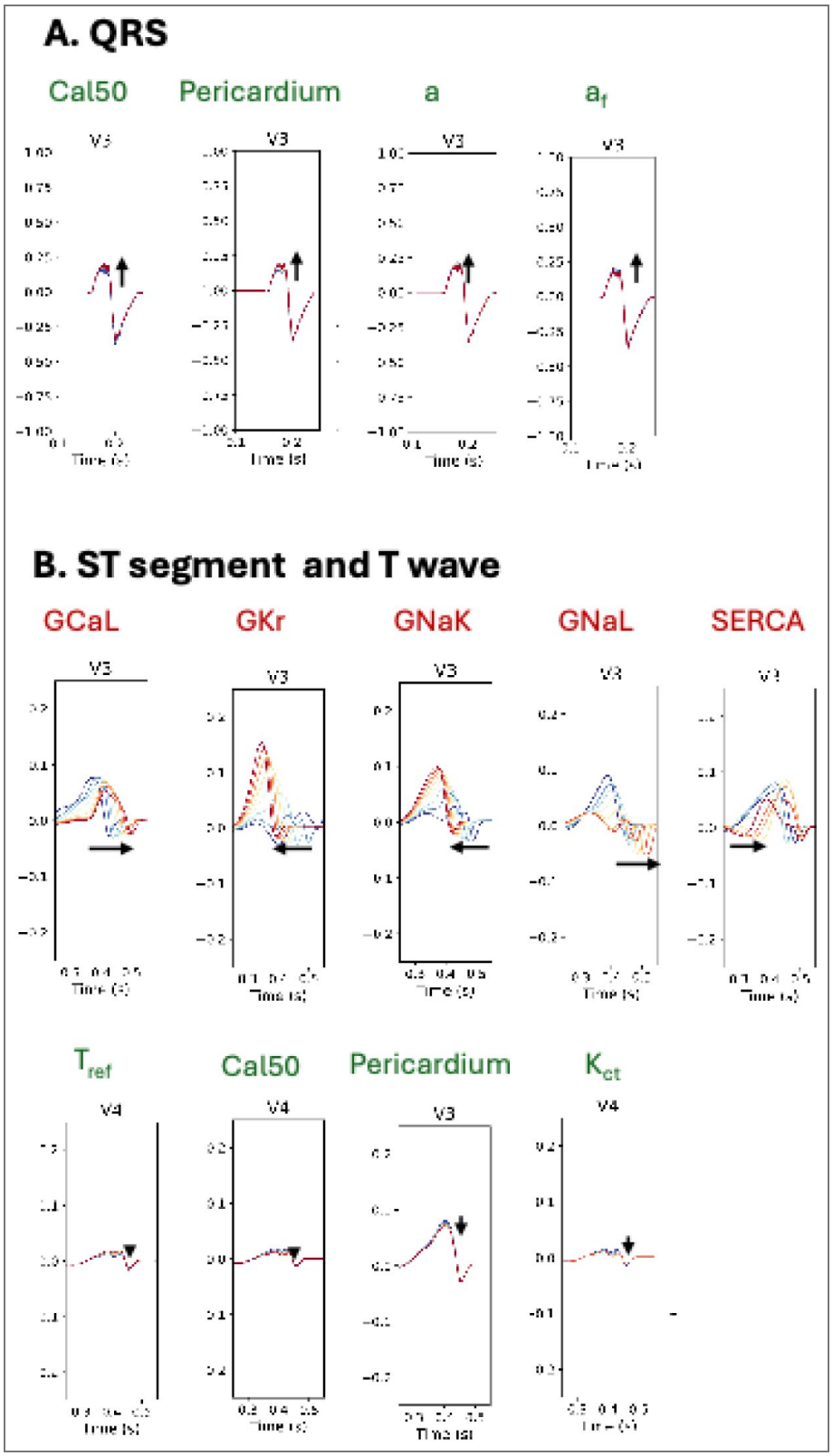

Figure A3. Of the parameters included in the analysis, the QRS section of the ECG showed minor sensitivity to variability in mechanical parameters (green labels) (A) while the ST and T wave segments of the ECG were strongly sensitivity to uncertainties in ionic conductances (red labels), and only showed minor sensitivity to some mechanical parameters (green labels) (B).

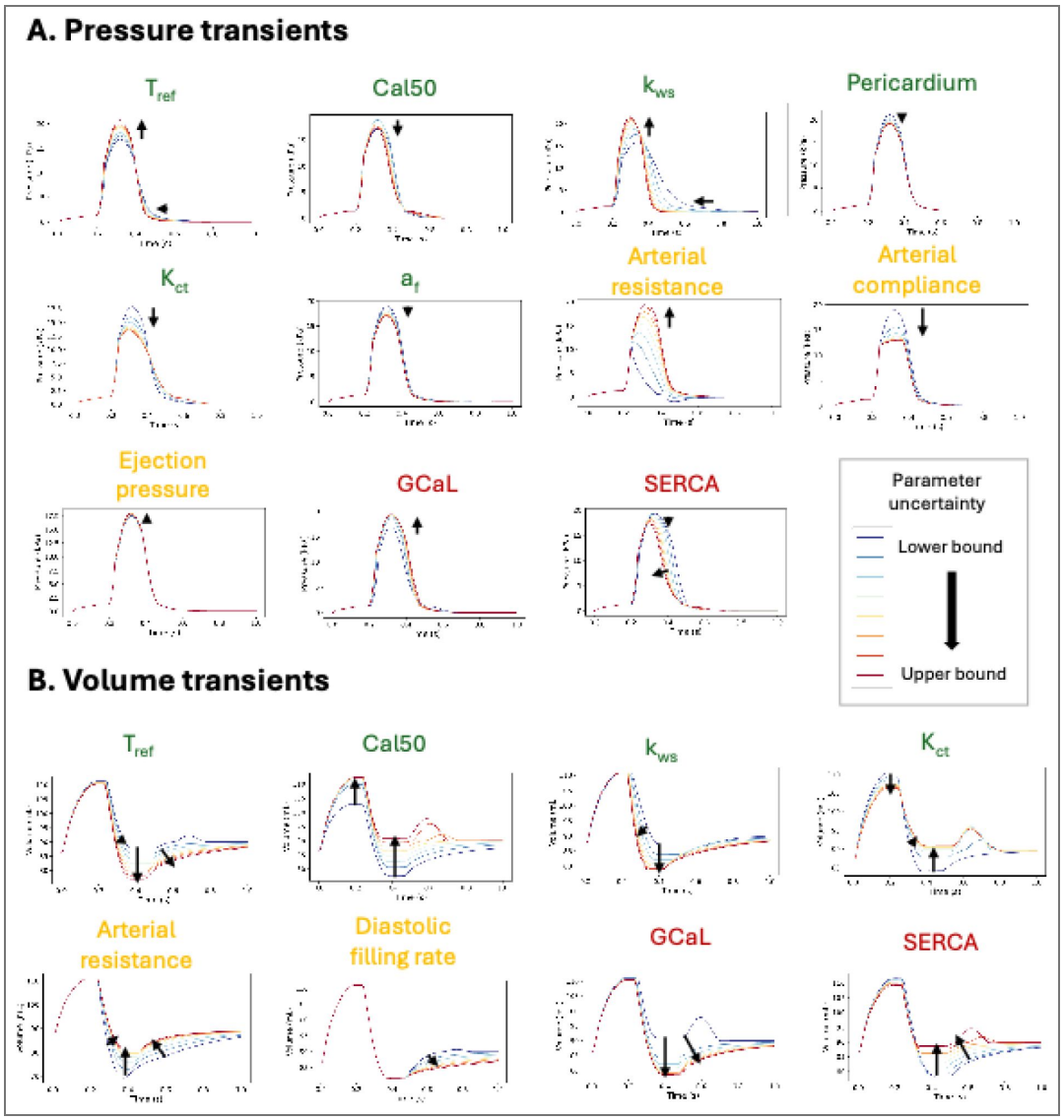

Figure A4. **Pressure (A) and volume (B) transients in response to parameter variability in mechanical properties (green), circulation (yellow), ionic conductances (red).**

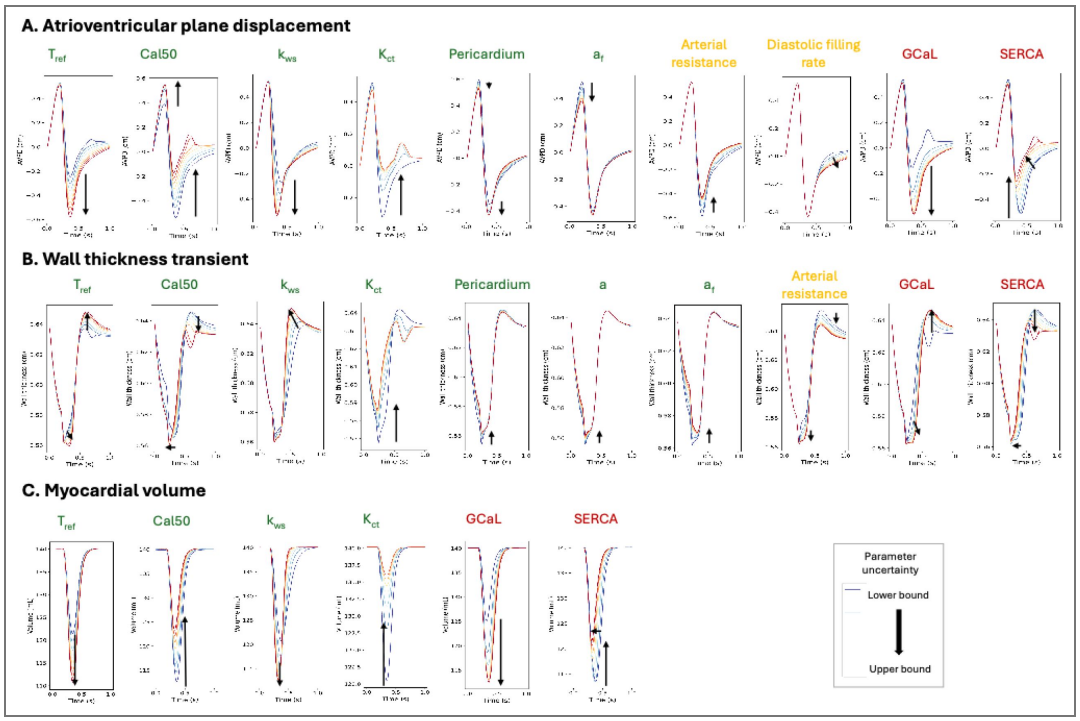

Figure A5. Key aspects of the ventricular deformation, including atrioventricular plane displacement, wall thickness changes, and myocardium volume changes were affected predominantly by mechanical parameters (green) and ionic conductance parameters (red), with weaker effects from circulatory parameters (yellow).

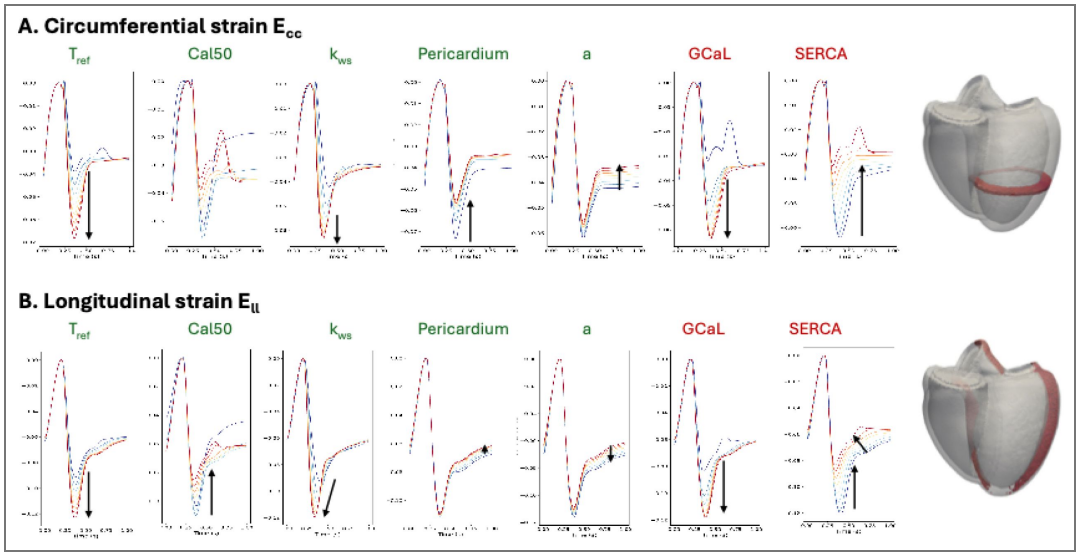

Figure A6. Sensitivity analysis in simulated strain transients were influenced by variability in mechanical (green), circulatory (yellow), and ionic conductance (red) parameters.

Additional information

Funding

Funder	Grant reference number	Author
Wellcome Trust (WT)	https://doi.org/10.35802/214290	Julia Camps Zhinuo Jenny Wang Blanca Rodriguez Maxx Holmes Ruben Doste Francesca Margara

Author ORCID iDs

Zhinuo Jenny Wang: https://orcid.org/0000-0001-5325-909X

References

1. **The American Society of Mechanical Engineers** (2018) VV40-Assessing Credibility of Computational Modeling through Verification and Validation Application to Medical Devices. ASME. https://www.asme.org/codes-standards/find-codes-standards/assessing-credibility-of-computational-modeling-through-verification-and-validation-application-to-medical-devices
2. **Niederer SA,** Sacks MS, Girolami M, Willcox K (2021) Scaling digital twins from the artisanal to the industrial. *Nat Comput Sci* **1**:313-320 https://doi.org/10.1038/s43588-021-00072-5 | PubMed
3. **Corral-Acero J,** et al. (2020) The 'Digital Twin' to enable the vision of precision cardiology. *Eur Heart J* **41**:4556-4564 https://doi.org/10.1093/eurheartj/ehaa159 | PubMed
4. **Sel K,** et al. (2024) Building Digital Twins for Cardiovascular Health: From Principles to Clinical Impact. *J Am Heart Assoc Cardiovasc Cerebrovasc Dis* **13**:e031981 https://doi.org/10.1161/jaha.123.031981 | PubMed
5. **Dasí A,** et al. (2022) In-silico drug trials for precision medicine in atrial fibrillation: From ionic mechanisms to electrocardiogram-based predictions in structurally-healthy human atria. *Front Physiol* **13** https://doi.org/10.3389/fphys.2022.966046 | PubMed
6. **Dasí A,** et al. (2024) In Silico TRials guide optimal stratification of ATrIal FIbrillation patients to Catheter Ablation and pharmacological medicaTION: the i-STRATIFICATION study. *EP Eur* **26**:euae150 https://doi.org/10.1093/europace/euae150 | PubMed
7. **Naderi H,** et al. (2023) Predicting left ventricular hypertrophy from the 12-lead electrocardiogram in the UK Biobank imaging study using machine learning. *Eur Heart J - Digit Health* **4**:316-324 https://doi.org/10.1093/ehjdh/ztad037 | PubMed
8. **Fedele M,** et al. (2023) A comprehensive and biophysically detailed computational model of the whole human heart electromechanics. *Comput Methods Appl Mech Eng* **410**:115983 https://doi.org/10.1016/j.cma.2023.115983
9. **Gerach T,** et al. (2021) Electro-Mechanical Whole-Heart Digital Twins: A Fully Coupled Multi-Physics Approach. *Mathematics* **9**:1247 https://doi.org/10.3390/math9111247
10. **Levrero-Florencio F,** et al. (2020) Sensitivity analysis of a strongly-coupled human-based electromechanical cardiac model: Effect of mechanical parameters on physiologically relevant biomarkers. *Comput Methods Appl Mech Eng* **361**:112762 https://doi.org/10.1016/j.cma.2019.112762 | PubMed
11. **Moss R,** Wülfers EM, Schuler S, Loewe A, Seemann G (2021) A Fully-Coupled Electro-Mechanical Whole-Heart Computational Model: Influence of Cardiac Contraction on the ECG. *Front Physiol* **12** https://doi.org/10.3389/fphys.2021.778872 | PubMed

12. **Zhou X,** et al. (2024) Clinical phenotypes in acute and chronic infarction explained through human ventricular electromechanical modelling and simulations. *eLife* **13** https://doi.org/10.7554/elife.93002 | PubMed
13. **Jie X,** Gurev V, Trayanova N (2010) Mechanisms of Mechanically Induced Spontaneous Arrhythmias in Acute Regional Ischemia. *Circ Res* **106**:185-192 https://doi.org/10.1161/circresaha.109.210864 | PubMed
14. **Keldermann RH,** Nash MP, Gelderblom H, Wang VY, Panfilov AV (2010) Electromechanical wavebreak in a model of the human left ventricle. *Am J Physiol-Heart Circ Physiol* **299**:H134-H143 https://doi.org/10.1152/ajpheart.00862.2009 | PubMed
15. **Margara F,** et al. (2022) Mechanism based therapies enable personalised treatment of hypertrophic cardiomyopathy. *Sci Rep* **12**:22501 https://doi.org/10.1038/s41598-022-26889-2 | PubMed
16. **Capuano E,** et al. (2024) Personalized computational electro-mechanics simulations to optimize cardiac resynchronization therapy. *Biomech Model Mechanobiol* **23**:1977-2004 https://doi.org/10.1007/s10237-024-01878-8 | PubMed
17. **Corral Acero J,** et al. (2024) Comprehensive characterization of cardiac contraction for improved post-infarction risk assessment. *Sci Rep* **14**:8951 https://doi.org/10.1038/s41598-024-59114-3 | PubMed
18. **Camps J,** et al. (2024) Digital twinning of the human ventricular activation sequence to Clinical 12-lead ECGs and magnetic resonance imaging using realistic Purkinje networks for in silico clinical trials. *Med Image Anal* **94**:103108 https://doi.org/10.1016/j.media.2024.103108 | PubMed
19. **Jung A,** Gsell MAF, Augustin CM, Plank G (2022) An Integrated Workflow for Building Digital Twins of Cardiac Electromechanics—A Multi-Fidelity Approach for Personalising Active Mechanics. *Mathematics* **10**:823 https://doi.org/10.3390/math10050823 | PubMed
20. **Trayanova NA,** Lyon A, Shade J, Heijman J (2024) Computational modeling of cardiac electrophysiology and arrhythmogenesis: toward clinical translation. *Physiol Rev* **104**:1265-1333 https://doi.org/10.1152/physrev.00017.2023 | PubMed
21. **Santiago A,** et al. (2022) Design and execution of a verification, validation, and uncertainty quantification plan for a numerical model of left ventricular flow after LVAD implantation. *PLOS Comput Biol* **18**:e1010141 https://doi.org/10.1371/journal.pcbi.1010141 | PubMed
22. **Arminio M,** Carbonaro D, Morbiducci U, Gallo D, Chiastra C (2024) Fluid-structure interaction simulation of mechanical aortic valves: a narrative review exploring its role in total product life cycle. *Front Med Technol* **6** https://doi.org/10.3389/fmedt.2024.1399729 | PubMed
23. **Tomek J,** et al. (2019) Development, calibration, and validation of a novel human ventricular myocyte model in health, disease, and drug block. *eLife* **8**:e48890 https://doi.org/10.7554/eLife.48890 | PubMed
24. **Land S,** et al. (2017) A model of cardiac contraction based on novel measurements of tension development in human cardiomyocytes. *J Mol Cell Cardiol* **106**:68-83 https://doi.org/10.1016/j.yjmcc.2017.03.008 | PubMed
25. **Passini E,** et al. (2017) Human In Silico Drug Trials Demonstrate Higher Accuracy than Animal Models in Predicting Clinical Pro-Arrhythmic Cardiotoxicity. *Front Physiol* **8** https://doi.org/10.3389/fphys.2017.00668 | PubMed
26. **Margara F,** et al. (2021) In-silico human electro-mechanical ventricular modelling and simulation for drug-induced pro-arrhythmia and inotropic risk assessment. *Prog Biophys Mol Biol* **159**:58-74 https://doi.org/10.1016/j.pbiomolbio.2020.06.007 | PubMed
27. **Campos JO,** Sundnes J, dos Santos RW, Rocha BM (2020) Uncertainty quantification and sensitivity analysis of left ventricular function during the full cardiac cycle. *Philos Trans R Soc Math Phys Eng Sci* **378**:20190381 https://doi.org/10.1098/rsta.2019.0381 | PubMed

28. **Rodero C,** et al. (2021) Linking statistical shape models and simulated function in the healthy adult human heart. *PLOS Comput Biol* **17**:e1008851 https://doi.org/10.1371/journal.pcbi.1008851 | PubMed

29. **Longobardi S,** et al. (2020) Predicting left ventricular contractile function via Gaussian process emulation in aortic-banded rats. *Philos Trans R Soc Math Phys Eng Sci* **378**:20190334 https://doi.org/10.1098/rsta.2019.0334 | PubMed

30. **Mirams GR,** Niederer SA, Clayton RH (2020) The fickle heart: uncertainty quantification in cardiac and cardiovascular modelling and simulation. *Philos Trans R Soc Math Phys Eng Sci* **378**:20200119 https://doi.org/10.1098/rsta.2020.0119 | PubMed

31. **Strocchi M,** et al. (2020) Simulating ventricular systolic motion in a four-chamber heart model with spatially varying robin boundary conditions to model the effect of the pericardium. *J Biomech* **101**:109645 https://doi.org/10.1016/j.jbiomech.2020.109645 | PubMed

32. **Strocchi M,** et al. (2023) Cell to whole organ global sensitivity analysis on a four-chamber heart electromechanics model using Gaussian processes emulators. *PLOS Comput Biol* **19**:e1011257 https://doi.org/10.1371/journal.pcbi.1011257 | PubMed

33. **Camps J,** et al. (2025) Harnessing 12-lead ECG and MRI data to personalise repolarisation profiles in cardiac digital twin models for enhanced virtual drug testing. *Med Image Anal* **100**:103361 https://doi.org/10.1016/j.media.2024.103361 | PubMed

34. **Roy CJ,** Oberkampf WL (2011) A comprehensive framework for verification, validation, and uncertainty quantification in scientific computing. *Comput Methods Appl Mech Eng* **200**:2131-2144 https://doi.org/10.1016/j.cma.2011.03.016

35. **Petersen SE,** et al. (2016) Reference ranges for cardiac structure and function using cardiovascular magnetic resonance (CMR) in Caucasians from the UK Biobank population cohort. *J Cardiovasc Magn Reson* **19**:18 https://doi.org/10.1186/s12968-017-0327-9 | PubMed

36. **Petersen SE,** et al. (2013) Imaging in population science: cardiovascular magnetic resonance in 100,000 participants of UK Biobank - rationale, challenges and approaches. *J Cardiovasc Magn Reson* **15**:1-10 https://doi.org/10.1186/1532-429x-15-46 | PubMed

37. **Littlejohns TJ,** et al. (2020) The UK Biobank imaging enhancement of 100,000 participants: rationale, data collection, management and future directions. *Nat Commun* **11**:2624 https://doi.org/10.1038/s41467-020-15948-9 | PubMed

38. **Nordsletten D,** et al. (2021) A viscoelastic model for human myocardium. *Acta Biomater* **135**:441-457 https://doi.org/10.1016/j.actbio.2021.08.036 | PubMed

39. **Holzapfel GA,** Ogden RW (2009) Constitutive modelling of passive myocardium: a structurally based framework for material characterization. *Philos Trans R Soc Math Phys Eng Sci* **367**:3445-3475 https://doi.org/10.1098/rsta.2009.0091 | PubMed

40. **Eriksson T,** Prassl A, Plank G, Holzapfel G (2013) Influence of myocardial fiber/sheet orientations on left ventricular mechanical contraction. *Math Mech Solids* **18**:592-606 https://doi.org/10.1177/1081286513485779

41. **Soares JS,** et al. (2017) Modeling of Myocardium Compressibility and its Impact in Computational Simulations of the Healthy and Infarcted Heart. In: Pop M, Wright GA (Eds). *Functional Imaging and Modelling of the Heart* Cham: Springer International Publishing. pp. 493-501 https://doi.org/10.1007/978-3-319-59448-4_47 | PubMed

42. **Lin DHS,** Yin FCP (1998) A Multiaxial Constitutive Law for Mammalian Left Ventricular Myocardium in Steady-State Barium Contracture or Tetanus. *J Biomech Eng* **120**:504-517 https://doi.org/10.1115/1.2798021 | PubMed

43. **Murch SD,** et al. (2015) Abnormal Right Ventricular Relaxation in Pulmonary Hypertension. *Pulm Circ* **5**:370-375 https://doi.org/10.1086/681268 | PubMed

44. **Pagoulatou S,** Stergiopulos N (2017) Evolution of aortic pressure during normal ageing: A model-based study. *PLOS One* **12**:e0182173 https://doi.org/10.1371/journal.pone.0182173 | PubMed

45. **Wright SP,** et al. (2017) Diastolic Pressure Difference to Classify Pulmonary Hypertension in the Assessment of Heart Transplant Candidates. *Circ Heart Fail* **10**:e004077 https://doi.org/10.1161/circheartfailure.117.004077 | PubMed

46. **Chung CS,** Karamanoglu M, Kovács SJ (2004) Duration of diastole and its phases as a function of heart rate during supine bicycle exercise. *Am J Physiol-Heart Circ Physiol* **287**:H2003-H2008 https://doi.org/10.1152/ajpheart.00404.2004 | PubMed

47. **Wang ZJ,** et al. (2018) Left Ventricular Diastolic Myocardial Stiffness and End-Diastolic Myofibre Stress in Human Heart Failure Using Personalised Biomechanical Analysis. *J Cardiovasc Transl Res* **11**:346-356 https://doi.org/10.1007/s12265-018-9816-y | PubMed

48. **Seed WA,** et al. (1984) Relationships between beat-to-beat interval and the strength of contraction in the healthy and diseased human heart. *Circulation* **70**:799-805 https://doi.org/10.1161/01.cir.70.5.799 | PubMed

49. **Pfaller MR,** et al. (2019) The importance of the pericardium for cardiac biomechanics: from physiology to computational modeling. *Biomech Model Mechanobiol* **18**:503-529 https://doi.org/10.1007/s10237-018-1098-4 | PubMed

50. **Doste R,** et al. (2019) A rule-based method to model myocardial fiber orientation in cardiac biventricular geometries with outflow tracts. *Int J Numer Methods Biomed Eng* **35**:e3185 https://doi.org/10.1002/cnm.3185 | PubMed

51. **Legrice IJ,** Hunter PJ, Smaill BH (1997) Laminar structure of the heart: a mathematical model. *Am J Physiol-Heart Circ Physiol* **272**:H2466-H2476 https://doi.org/10.1152/ajpheart.1997.272.5.h2466 | PubMed

52. **De Marco M,** et al. (2017) Influence of Left Ventricular Stroke Volume on Incident Heart Failure in a Population with Preserved Ejection Fraction (From the Strong Heart Study). *Am J Cardiol* **119**:1047-1052 https://doi.org/10.1016/j.amjcard.2016.12.011

53. **Nielles-Vallespin S,** et al. (2017) Assessment of Myocardial Microstructural Dynamics by In Vivo Diffusion Tensor Cardiac Magnetic Resonance. *J Am Coll Cardiol* **69**:661-676 https://doi.org/10.1016/j.jacc.2016.11.051 | PubMed

54. **Carlsson M,** Ugander M, Mosén H, Buhre T, Arheden H (2007) Atrioventricular plane displacement is the major contributor to left ventricular pumping in healthy adults, athletes, and patients with dilated cardiomyopathy. *Am J Physiol-Heart Circ Physiol* **292**:H1452-H1459 https://doi.org/10.1152/ajpheart.01148.2006 | PubMed

55. **Moulin K,** et al. (2021) Myofiber strain in healthy humans using DENSE and cDTI. *Magn Reson Med* **86**:277-292 https://doi.org/10.1002/mrm.28724 | PubMed

56. **Santiago A,** et al. (2018) Fully coupled fluid-electro-mechanical model of the human heart for supercomputers. *Int J Numer Methods Biomed Eng* **34**:e3140 https://doi.org/10.1002/cnm.3140 | PubMed

57. **Taggart P,** et al. (2000) Inhomogeneous Transmural Conduction During Early Ischaemia in Patients with Coronary Artery Disease. *J Mol Cell Cardiol* **32**:621-630 https://doi.org/10.1006/jmcc.2000.1105 | PubMed

58. **Myerburg RJ,** Nilsson K, Gelband H (1972) Physiology of Canine Intraventricular Conduction and Endocardial Excitation. *Circ Res* **30**:217-243 https://doi.org/10.1161/01.res.30.2.217 | PubMed

59. **Young WJ,** et al. (2021) Genetically Determined Serum Calcium Levels and Markers of Ventricular Repolarization: A Mendelian Randomization Study in the UK Biobank. *Circ Genomic Precis Med* **14**:e003231 https://doi.org/10.1161/circgen.120.003231 | PubMed

60. **Berul CI,** Sweeten TL, Dubin AM, Shah MJ, Vetter VL (1994) Use of the rate-corrected JT interval for prediction of repolarization abnormalities in children. *Am J Cardiol* **74**:1254-1257 https://doi.org/10.1016/0002-9149(94)90558-4 | PubMed

61. **Zulqarnain MA,** Qureshi WT, O'Neal WT, Shah AJ, Soliman EZ (2015) Risk of Mortality Associated with QT and JT Intervals at Different Levels of QRS Duration (from the Third National Health and Nutrition Examination Survey [NHANES III]). *Am J Cardiol* **116**:74-78 https://doi.org/10.1016/j.amjcard.2015.03.038 | PubMed

62. **Ramírez J,** et al. (2022) ECG T-Wave Morphologic Variations Predict Ventricular Arrhythmic Risk in Low- and Moderate-Risk Populations. *J Am Heart Assoc* **11**:e025897 https://doi.org/10.1161/jaha.121.025897 | PubMed

63. **Panikkath R,** et al. (2011) Prolonged Tpeak-to-Tend Interval on the Resting ECG Is Associated With Increased Risk of Sudden Cardiac Death. *Circ Arrhythm Electrophysiol* **4**:441-447 https://doi.org/10.1161/circep.110.960658 | PubMed

64. **Sugrue A,** et al. (2017) Utility of T-wave amplitude as a non-invasive risk marker of sudden cardiac death in hypertrophic cardiomyopathy. *Open Heart* **4**:e000561 https://doi.org/10.1136/openhrt-2016-000561 | PubMed

65. **Helmy H,** Abdel-Galeel A, Taha Kishk Y, Mohammed Sleem K (2017) Correlation of corrected QT dispersion with the severity of coronary artery disease detected by SYNTAX score in non-diabetic patients with STEMI. *Egypt Heart J* **69**:111-117 https://doi.org/10.1016/j.ehj.2016.12.001 | PubMed

66. **Joseph J,** et al. (2016) QRS Duration Is a Predictor of Adverse Outcomes in Heart Failure With Preserved Ejection Fraction. *JACC Heart Fail* **4**:477-486 https://doi.org/10.1016/j.jchf.2016.02.013 | PubMed

67. **Nambiar L,** Li A, Howard A, LeWinter M, Meyer M (2018) Left ventricular end-diastolic volume predicts exercise capacity in patients with a normal ejection fraction. *Clin Cardiol* **41**:628-633 https://doi.org/10.1002/clc.22928 | PubMed

68. **Kato M,** et al. (2020) Left Ventricular End-Systolic Volume Is a Reliable Predictor of New-Onset Heart Failure with Preserved Left Ventricular Ejection Fraction. *Cardiol Res Pract* **2020**:3106012 https://doi.org/10.1155/2020/3106012 | PubMed

69. **Göransson C,** Vejlstrup N, Carlsen J (2022) Clinically important changes in right ventricular volume and function in pulmonary arterial hypertension assessed with cardiac magnetic resonance imaging. *Pulm Circ* **12**:e12097 https://doi.org/10.1002/pul2.12097 | PubMed

70. **Tedford RJ,** et al. (2013) Right Ventricular Dysfunction in Systemic Sclerosis–Associated Pulmonary Arterial Hypertension. *Circ Heart Fail* **6**:953-963 https://doi.org/10.1161/circheartfailure.112.000008 | PubMed

71. **Edward J,** Banchs J, Parker H, Cornwell W (2023) Right ventricular function across the spectrum of health and disease. *Heart* **109**:349-355 https://doi.org/10.1136/heartjnl-2021-320526 | PubMed

72. **Hendriks T,** et al. (2019) Effect of Systolic Blood Pressure on Left Ventricular Structure and Function. *Hypertension* **74**:826-832 https://doi.org/10.1161/hypertensionaha.119.12679 | PubMed

73. **Batzner A,** et al. (2024) Non-invasive estimation of left ventricular systolic peak pressure: a prerequisite to calculate myocardial work in hypertrophic obstructive cardiomyopathy. *Eur Heart J - Cardiovasc Imaging* **25**:213-219 https://doi.org/10.1093/ehjci/jead236 | PubMed

74. **Oliver RM,** Peacock AJ, Challenor VF, Fleming JS, Waller DG (1991) The effect of acute hypoxia on right ventricular function in healthy adults. *Int J Cardiol* **31**:235-241 https://doi.org/10.1016/0167-5273(91)90221-a | PubMed

75. **McDonagh TA,** et al. (2021) 2021 ESC Guidelines for the diagnosis and treatment of acute and chronic heart failure: Developed by the Task Force for the diagnosis and treatment of acute and chronic heart failure of the European Society of Cardiology (ESC) With the special contribution of the Heart Failure Association (HFA) of the ESC. *Eur Heart J* **42**:3599-3726 https://doi.org/10.1093/eurheartj/ehab670 | PubMed

76. **Ginks MR,** et al. (2011) Relationship between intracardiac impedance and left ventricular contractility in patients undergoing cardiac resynchronization therapy. *EP Eur* **13**:984-991 https://doi.org/10.1093/europace/eur055 | PubMed

77. **Ostadal P,** Vondrakova D, Krüger A, Janotka M, Naar J (2019) Continual measurement of arterial dP/dtmax enables minimally invasive monitoring of left ventricular contractility in patients with acute heart failure. *Crit Care* **23**:364 https://doi.org/10.1186/s13054-019-2654-8 | PubMed

78. **Zeidan Z,** et al. (2003) Analysis of global systolic and diastolic left ventricular performance using volume-time curves by real-time three-dimensional echocardiography. *J Am Soc Echocardiogr* **16**:29-37 https://doi.org/10.1067/mje.2003.40 | PubMed

79. **Hammermeister KE,** Brooks RC, Warbasse JR (1974) The Rate of Change of Left Ventricular Volume in Man. *Circulation* **49**:729-738 https://doi.org/10.1161/01.cir.49.4.729 | PubMed

80. **König CS,** Atherton M, Cavazzuti M, Gomm C, Ramachandran S (2021) The association of peak systolic velocity in the carotid artery with coronary heart disease: A study based on portable ultrasound. *Proc Inst Mech Eng* **235**:663-675 https://doi.org/10.1177/09544119211000482 | PubMed

81. **Ohno M,** Cheng CP, Little WC (1994) Mechanism of altered patterns of left ventricular filling during the development of congestive heart failure. *Circulation* **89**:2241-2250 https://doi.org/10.1161/01.cir.89.5.2241 | PubMed

82. **Land S,** et al. (2015) Verification of cardiac mechanics software: benchmark problems and solutions for testing active and passive material behaviour. *Proc R Soc Math Phys Eng Sci* **471**:20150641 https://doi.org/10.1098/rspa.2015.0641 | PubMed

83. **Attar R,** et al. (2019) Quantitative CMR population imaging on 20,000 subjects of the UK Biobank imaging study: LV/RV quantification pipeline and its evaluation. *Med Image Anal* **56**:26-42 https://doi.org/10.1016/j.media.2019.05.006 | PubMed

84. **Rodrigues JCL,** et al. (2017) Hypertensive heart disease versus hypertrophic cardiomyopathy: multi-parametric cardiovascular magnetic resonance discriminators when end-diastolic wall thickness ≥ 15 mm. *Eur Radiol* **27**:1125-1135 https://doi.org/10.1007/s00330-016-4468-2 | PubMed

85. **Dong SJ,** et al. (1994) Left ventricular wall thickness and regional systolic function in patients with hypertrophic cardiomyopathy. A three-dimensional tagged magnetic resonance imaging study. *Circulation* **90**:1200-1209 https://doi.org/10.1161/01.cir.90.3.1200 | PubMed

86. **Mignot A,** et al. (2010) Global Longitudinal Strain as a Major Predictor of Cardiac Events in Patients with Depressed Left Ventricular Function: A Multicenter Study. *J Am Soc Echocardiogr* **23**:1019-1024 https://doi.org/10.1016/j.echo.2010.07.019 | PubMed

87. **Smiseth OA,** Torp H, Opdahl A, Haugaa KH, Urheim S (2016) Myocardial strain imaging: how useful is it in clinical decision making?. *Eur Heart J* **37**:1196-1207 https://doi.org/10.1093/eurheartj/ehv529 | PubMed

88. **Zhang KW,** et al. (2014) Strain Improves Risk Prediction Beyond Ejection Fraction in Chronic Systolic Heart Failure. *J Am Heart Assoc* **3**:e000550 https://doi.org/10.1161/jaha.113.000550 | PubMed

89. **Borlaug BA,** Kass DA (2006) Mechanisms of Diastolic Dysfunction in Heart Failure. *Trends Cardiovasc Med* **16**:273-279 https://doi.org/10.1016/j.tcm.2006.05.003 | PubMed

90. **Coveney S,** et al. (2021) Bayesian Calibration of Electrophysiology Models Using Restitution Curve Emulators. *Front Physiol* **12** https://doi.org/10.3389/fphys.2021.693015 | PubMed

91. **Favino M,** et al. (2016) Impact of mechanical deformation on pseudo-ECG: a simulation study. *EP Eur* **18**:iv77-iv84 https://doi.org/10.1093/europace/euw353 | PubMed

92. **Zingaro A,** et al. (2024) An electromechanics-driven fluid dynamics model for the simulation of the whole human heart. *J Comput Phys* **504**:112885 https://doi.org/10.1016/j.jcp.2024.112885

93. **Aróstica R,** et al. (2025) A software benchmark for cardiac elastodynamics. *Comput Methods Appl Mech Eng* **435**:117485 https://doi.org/10.1016/j.cma.2024.117485

94. **Kumar V,** et al. (2021) Cardiac MRI demonstrates compressibility in healthy myocardium but not in myocardium with reduced ejection fraction. *Int J Cardiol* **322**:278-283 https://doi.org/10.1016/j.ijcard.2020.08.087 | PubMed

95. **Miller L,** Penta R (2025) Homogenized multiscale modelling of an electrically active double poroelastic material representing the myocardium. *Biomech Model Mechanobiol* **24**:635-662 https://doi.org/10.1007/s10237-025-01931-0 | PubMed

96. **LeGrice IJ,** Takayama Y, Covell JW (1995) Transverse Shear Along Myocardial Cleavage Planes Provides a Mechanism for Normal Systolic Wall Thickening. *Circ Res* **77**:182-193 https://doi.org/10.1161/01.res.77.1.182 | PubMed

97. **Zheng Y,** et al. (2023) Effects of myocardial sheetlet sliding on left ventricular function. *Biomech Model Mechanobiol* **22**:1313-1332 https://doi.org/10.1007/s10237-023-01721-6 | PubMed

98. **Stassen J,** Jogani S, Schroyens M (2021) Strain reversus revealing constrictive pericarditis. *Eur Heart J - Cardiovasc Imaging* **22**:e14 https://doi.org/10.1093/ehjci/jeaa225 | PubMed

99. **Hadjicharalambous M,** et al. (2021) Investigating the reference domain influence in personalised models of cardiac mechanics. *Biomech Model Mechanobiol* **20**:1579-1597 https://doi.org/10.1007/s10237-021-01464-2 | PubMed

100. **Kallhovd S,** Sundnes J, Wall ST (2019) Sensitivity of stress and strain calculations to passive material parameters in cardiac mechanical models using unloaded geometries. *Comput Methods Biomech Biomed Engin* **22**:664-675 https://doi.org/10.1080/10255842.2019.1579312 | PubMed

101. **Wang ZJ,** et al. (2020) Efficient estimation of load-free left ventricular geometry and passive myocardial properties using principal component analysis. *Int J Numer Methods Biomed Eng* **36**:e3313 https://doi.org/10.1002/cnm.3313 | PubMed

102. **Marx L,** et al. (2022) Robust and efficient fixed-point algorithm for the inverse elastostatic problem to identify myocardial passive material parameters and the unloaded reference configuration. *J Comput Phys* **463**:111266 https://doi.org/10.1016/j.jcp.2022.111266 | PubMed

103. **Nikou A,** et al. (2016) Effects of using the unloaded configuration in predicting the in vivo diastolic properties of the heart. *Comput Methods Biomech Biomed Engin* **19**:1714-1720 https://doi.org/10.1080/10255842.2016.1183122 | PubMed

104. **Tang D,** et al. (2016) Patient-Specific MRI-Based Right Ventricle Models Using Different Zero-Load Diastole and Systole Geometries for Better Cardiac Stress and Strain Calculations and Pulmonary Valve Replacement Surgical Outcome Predictions. *PLOS One* **11**:e0162986 https://doi.org/10.1371/journal.pone.0162986 | PubMed

105. **Genet M,** et al. (2015) Heterogeneous growth-induced prestrain in the heart. *J Biomech* **48**:2080-2089 https://doi.org/10.1016/j.jbiomech.2015.03.012 | PubMed

106. **Omens JH,** Fung YC (1990) Residual strain in rat left ventricle. *Circ Res* **66**:37-45 https://doi.org/10.1161/01.res.66.1.37 | PubMed

107. **Arts T,** Delhaas T, Bovendeerd P, Verbeek X, Prinzen FW (2005) Adaptation to mechanical load determines shape and properties of heart and circulation: the CircAdapt model. *Am J Physiol-Heart Circ Physiol* **288**:H1943-H1954 https://doi.org/10.1152/ajpheart.00444.2004 | PubMed

108. **Fritz T,** Wieners C, Seemann G, Steen H, Dössel O (2014) Simulation of the contraction of the ventricles in a human heart model including atria and pericardium. *Biomech Model Mechanobiol* **13**:627-641 https://doi.org/10.1007/s10237-013-0523-y | PubMed

109. **Scardulla F,** Rinaudo A, Pasta S, Scardulla C (2015) Mechanics of pericardial effusion: A simulation study. *Proc Inst Mech Eng* **229**:205-214 https://doi.org/10.1177/0954411915574012 | PubMed

110. **Miller R,** et al. (2021) An Implementation of Patient-Specific Biventricular Mechanics Simulations With a Deep Learning and Computational Pipeline. *Front Physiol* **12** https://doi.org/10.3389/fphys.2021.716597 | PubMed

111. **Brown AL,** et al. (2025) Personalized biventricular mechanics and sensitivity to model morphology. *bioRxiv* 2025.12.11.693778 https://doi.org/10.64898/2025.12.11.693778

Peer reviews

Reviewer #1 (Public review):

Summary:

The study by Wang et al. investigates cardiac electromechanical modeling and simulation techniques, focusing on the calibration and validation of ventricular models according to ASME V&V40 standards. The researchers aim to calibrate model parameters to align with key biomarkers such as QRS duration and left ventricular ejection fraction and validate the model against independent measurements such as displacement and strain metrics. The authors also examine the impact of parameter variations on deformation, ejection fraction, strains and other biomarkers. The overarching aim of the study is to give credibility to the underlying computational electromechanics framework as a step towards the cardiac Digital Twin vision.

Strengths:

(1) The study presents a solid validation strategy for cardiac models based on independent data.

(2) It integrates electrophysiological, mechanical, and hemodynamic biomarkers for sensitivity analysis and calibration.

Weaknesses and Limitations:

(1) Model Assumptions: The study relies on several simplified modeling assumptions that do not reflect the current state-of-the-art:

a) Isotropic scaling of the ventricular mesh to generate an unloaded reference geometry.

b) Simplified afterload and preload models that do not consistently capture the full range of physiological responses.

c) Simplified epicardial boundary conditions.

These limitations are appropriately acknowledged and discussed by the authors in a dedicated Limitations section.

(2) Numerical Framework:

a) The numerical framework used for the mechanical part of the model may be susceptible to locking effects that could contribute to artificially stiff and less contractile behavior. This is indicated by a ten-fold scaling of the peak active contractile force parameter relative to literature values and notable sensitivity of the model to the tissue compressibility parameter. While - as acknowledged by the authors - part of this can be attributed to simplified modeling choices, other comparable studies have not reported similar issues.

b) The human electrophysiology model is not described in enough detail. Currently, it is not mentioned in the manuscript that an Eikonal model was used to compute activation times on the endocardial surface to be robust against coarse mesh resolutions.

(3) Geometrical model and digital twin: The model presented combines anatomical data, electrical measurements, and physiological reference values from different individuals or population averages, rather than being derived from a single patient. The authors have appropriately moderated their claims in the revision, framing the work as a step towards the cardiac Digital Twin vision rather than asserting that the model itself constitutes a digital twin.

(4) Calibration procedure: The description of the calibration procedure has been substantially improved in the revision. The authors now provide explicit rationale for each calibration step and clarify that the procedure targets multiple physiological biomarkers in sequence. Verification that the calibrated model produces physiological cellular dynamics, including intracellular calcium transients, is now provided. The revised manuscript also shows the simulated electrocardiogram alongside population reference ranges, which partially addresses the question of calibration quality. However, a direct comparison of the simulated electrocardiogram with the individual measured signal used for calibration is not provided, which would give a more stringent and direct assessment of how well that specific calibration target was achieved.

Comments on revised version.

The revision represents a genuine improvement. The calibration procedure is now more transparently described, physiological cellular dynamics are verified, the digital twin framing has been appropriately moderated to reflect a step towards that vision rather than a claim of having achieved it, and an expanded limitations section identifies where the framework falls short.

Several of the concerns raised in the first round have been addressed, but some issues remain:

The model still requires a ten-fold scaling of the peak active contractile force relative to literature values, and the imbalance between left and right ventricular output persists, along with non-physiological right ventricular pressures and ejection fraction. These are partly fundamental limitations of the current modelling approach that may not be fully resolvable within the scope of this paper, and the authors are to be credited for acknowledging them. However, they do constrain the conclusions that can be drawn about the credibility of the framework for reproducing healthy cardiac physiology.

The population-averaged reference dataset and the calibration and validation framework remain contributions of value to the community, and the revised limitations section adds useful transparency about the current state of the art.

https://doi.org/10.7554/eLife.106555.2.sa2

Reviewer #2 (Public review):

The authors present an interesting study on calibrating and validating a biventricular cardiac electromechanical model. This is an important contribution, but some questions remain about the quantitative validation and verification aspects of the study.

Major comments:

(1) The title and paper stress the importance of validation on several occasions. However, the actual validation performed is limited to the section in lines 427-439. Furthermore, it is entirely qualitative, making assessing the model's quality difficult. Most of the paper is focused on sensitivity analysis, which is also interesting but unrelated to validation. Can you include a quantitative comparison with deformation biomarkers? E.g., spatially quantify

strain differences between simulation and in vivo data, or overlay the current configuration of the geometry with MRI in various views, and calculate a displacement error norm.

(2) You mention the ASME V&V40 standards throughout your paper. Yet, you only address the "second V" validation, ignoring the "first V" verification. How did you ensure that your computational models are implemented correctly?

(3) All parameters discussed in this publication are physical parameters. What is the sensitivity of your model outputs concerning computational parameters?

Comments on revised version.

The authors have addressed my prior comments

https://doi.org/10.7554/eLife.106555.2.sa1

Author response:

The following is the authors' response to the original reviews.

We greatly appreciate the reviewers for their efforts in reviewing our manuscript. We highlight that the key contributions of our paper are to provide a framework for calibration and validation of high-fidelity cardiac electromechanical models based on a diverse compilation of clinical datasets, and that we provide one example of such an evaluation of our own baseline electromechanical model. The comments raised by the reviewers were chiefly focused on the second goal, which is our specific model and the outcomes of the evaluation process, rather than on the evaluation framework itself. As such, we have made improvements to our model implementation and to provide additional confidence in our specific modelling framework through this review process. Specifically, we have strengthened the verification component of this evaluation, provided additional quantitative measures, and included a more in-depth discussion of the remaining limitations in our modelling framework. We hope that the updated version of the manuscript and our efforts to improve it are well-received by our reviewers and editors, as well as by the modelling and simulation community at large.

> ***eLife Assessment***
>
> *This is a potentially important study that explores the relevant range of parameter values for calibration and validation of cardiac electromechanics in ventricular models. Although much of the work presented is solid, the evidence provided to support the authors' key scientific claims is incomplete, especially as it relates to the emphasis on standardized validation and verification approaches. Notably, the level of model personalization presented in this work falls short of the threshold for what could reasonably be called a "digital twin", even by the relatively relaxed standards that have emerged in computational physiology and related fields in recent years.*

We appreciate the eLife assessment for identifying the potential importance of our study. Regarding the threshold for 'digital twin', we note that a cardiac digital twin is envisioned as a patient-specific computational model of the heart, personalised from multi-modal clinical data and continuously updated to support diagnosis, prognosis, and treatment planning, which is a goal that to our knowledge no published electromechanical study has simultaneously fulfilled. It is for this reason that the community refers to the 'digital twin vision' rather than its realisation, and we adopt this framing consistently throughout the manuscript.

The primary contribution of this manuscript is the framework: a systematic application of ASME V&V40 standards to a fully coupled electromechanical model, spanning electrical,

mechanical, and haemodynamic biomarkers within a single study. In our revision, we have clarified that the model evaluation presented here is an example application of that framework, which was designed not to certify a model as complete, but to provide a transparent audit of current capability that identifies where confidence is established and where further development is needed. We have updated the title and language throughout the manuscript to reflect this framing consistently.

> ***Public Reviews:***
>
> ***Reviewer #1 (Public review):***
>
> *Summary:*
>
> *The study by Wang et al. investigates cardiac electromechanical modeling and simulation techniques, focusing on the calibration and validation of ventricular models according to ASME V&V40 standards. The researchers aim to calibrate model parameters to align with key biomarkers such as QRS duration and left ventricular ejection fraction, and validate the model against independent measurements such as displacement and strain metrics. The authors also examine the impact of parameter variations on deformation, ejection fraction, strains, and other biomarkers. The overarching aim of the study is to give "credibility to the underlying computational electromechanics framework" and to "pave the way towards credible cardiac electromechanical Digital Twins."*
>
> *Strengths:*
>
> *(1) The study presents a solid validation strategy for cardiac models based on independent data.*
>
> *(2) It integrates electrophysiological, mechanical, and hemodynamic biomarkers for sensitivity analysis and calibration.*
>
> *Weaknesses and Limitations:*
>
> *(1) Model Assumptions: The study employs simplified modeling assumptions that are not state-of-the-art, e.g.,*
>
> *(a) Isotropic scaling of the mesh to generate an unloaded reference geometry.*
>
> *(b) Simple afterload and preload models that fail to produce physiological results.*
>
> *(c) Simplified epicardial boundary conditions.*

While our model was able to broadly achieve physiological behaviour based on the calibration and validation datasets, it also contains several simplifications that can be expanded with more sophisticated techniques to allow explorations in specific areas. We have added a dedicated Limitations subsection to the Discussion section of the manuscript to address these and to provide references to relevant studies.

> *(2) Numerical Framework:*
>
> *(a) The mesh resolution and/or the numerical framework used for the mechanical part appears to suffer from known numerical artifacts (locking effects), leading to overly stiff or inaccurate behavior in finite element analysis. This results in an artificially stiff response to deformation, which is compensated by setting active contraction to ten times the value reported in the literature. The authors attribute this to limitations in using ex vivo tissue measurements to represent in vivo function, although similar issues were not observed in previous works.*

We thank the reviewer for raising this point and have investigated it carefully. We have added a verification section as well as discussions to the manuscript to more comprehensively discuss this point. In short, through various tests against benchmark (Land) and comparing stress-strain curves in cube simulations with the same mesh resolution, we could not identify evidence of volumetric locking effects. The elevation in contractile force was also necessary in a simplified ellipsoid version of the model in a previous publication [ref 7, Levrero-Florencio, et al. 2020]. We note that these benchmarks were performed in the incompressible transversely isotropic regime; whether analogous locking effects exist in the dynamic orthotropic active contraction framework used in the full biventricular simulations remains an open question, which we have identified as a priority for future benchmarking, for example against the Arostica et al. 2025 benchmark.

We agree that the explanation of this as *ex vivo* vs *in vivo* difference in contractile force is too simple, and other contributing factors are better understood through comparison with similar studies in the field. Strocchi et al. (2023) used a four-chamber model with explicit atrial mechanics, and in her history matching varied Tref within +- 33-55% of a reference value of 120-150 kPa, targeting a peak active tension of 160 +- 15 kPa, which was a considerably more modest adjustment than applied here, likely reflecting differences in model geometry, pericardial constraint, and circulatory model between the two studies. Gerach et al. (2021, Mathematics) applied manual parameter adjustments informed by *in vivo* active tension measurements of 120 – 150 kPa and achieved ejection fractions of approximately 63%; however, they reported that systolic pressures in both ventricles were too high for a healthy heart, and similarly reported elevated peak ejection rates compared to MRI measurements, a difficulty we also encountered. Notably, Gerach et al., report that atrial contraction contributes approximately 11-13% of end-diastolic volume, which in a biventricular-only model would directly reduce the achievable LVEF and necessitate compensating adjustments to active tension. Zingaro et al. (2024, Journal of Computational Physics), using an alternative active tension model (RDQ20), similarly found it necessary to increase contractility parameter (a_XB) to achieve sufficient ejection, and explicitly report that no single parameter configuration simultaneously achieved physiological peak ejection rate and LVEF, a fundamental tension we also encountered. Together, these comparisons suggest that the elevated Tref in our model most likely reflects a combination of the absence of atrial filling, simplifications in pericardial constraint, and the lack of poroelastic behaviour, rather than volumetric locking alone. Additional investigations are needed as explained in the manuscript, and these factors are identified as open priorities for future development within our framework.

We added a comparison with these three studies to the discussion section of the manuscript and have updated the limitations section to reflect this more nuanced account of the factors contributing to the elevated active tension scaling. Further work will be required to address these points.

> *(b) Further, the authors employ the monodomain model for the simulation of the electrical excitation and relaxation on a relatively coarse grid with an approximate edge length of 1mm. This resolution is known to be insufficient for reliable results in organ-scale electrophysiology modeling.*

Our ECG simulations are robust against coarse mesh resolutions since we use an Eikonal solution to prescribe the activation times on the endocardial surface and we tune the diffusivity parameters in the model such that the correct conduction velocities are reached, as performed in Camps et al. (2024) (ref 33) using the tuneCV tool in monoAlg3D (*https://github.com/rsachetto/MonoAlg3D_C/tree/master/scripts/tuneCV*), which is similar to the tool in openCARP (described here: *https://opencarp.org/documentation/examples/02_ep_tissue/03a_study_prep_tunecv*).

While this mesh resolution may not be sufficient for simulations of more complex behaviour, such as re-entry and fibrillation patterns, it is sufficient for simulations of ECGs in this study. We have noted this in the methods section.

> *(3) Geometrical model and digital twin: The geometrical model, taken from a public cohort and calibrated to an ECG of another individual along with population-averaged values from a databank (UK Biobank), and unrelated measurements from surgical procedures, can hardly be considered a digital twin. Further, validation of the model was then performed against data from yet another cohort.*

We thank the reviewer for this point and welcome the opportunity to clarify our dataset choices. The use of multiple data sources was a deliberate methodological decision. While an ideal dataset for electromechanical model evaluation would combine full biventricular geometry, 12-lead ECG, invasive pressure measurements, and myocardial strain data from a single individual, no such dataset currently exists in the public domain, and acquiring it routinely would be impractical in clinical settings. Multi-source integration therefore reflects the realistic deployment scenario for future clinical translation of these tools.

The specific choice of geometry was principled: the mesh associated with the ECG dataset that was available to us was truncated at the base due to the clinical acquisition protocol, which would have prevented physiologically realistic basal boundary conditions. The female Rodero geometry we chose provides full ventricular coverage and was selected on that basis.

Demonstrating that a coherent, systematically evaluated framework can be constructed from compiled multi-modal data is itself a contribution because it makes the tools accessible to the wider community without requiring a single ideally acquired dataset.

> *(4) Calibration procedure: There are apparent flaws in the calibration procedure, or it is not described in sufficient detail. The authors dedicate significant effort to motivating parameter ranges, but in the end they use mostly other parameters for the calibration process, aiming to maximize left ventricular ejection fraction. It is not clear whether the chosen parameters result in, e.g., physiological calcium traces or calibrated parameters that are within physiological ranges.*

Thank you for raising this point, which we have now clarified in the manuscript. The parameters that were chosen for the calibration process were based on the results of the sensitivity analyses.

In addition, we have supplemented results Figure 1 with a subfigure F showing that the calcium transient and action potential durations fall within physiological ranges after calibration.

> *(5) Goodness of fits, e.g., a direct comparison of the measured and the simulated ECG, are not provided to assess calibration quality.*

The calibrated model achieves QRS duration of 89 ms and QT interval of 360 ms, both of which fall within the healthy reference ranges compiled in Table 2, providing a biomarker-level assessment of calibration quality (Figure 1A). A full quantitative goodness of fit analysis of the simulated ECG morphology was performed following the methodology of Camps et al. [52], in which the same beat-averaged ECG was processed; we direct the reader to that work for full details rather than reproducing the analysis here.

> *(6) Due to these limitations and weaknesses, the authors fall short of achieving some of their goals, particularly establishing credibility for the underlying computational framework and in reproducing healthy pressure-volume loops, and in achieving*

> *physiological simulations while using physiological or reported ranges for the calibrated parameters.*
>
> *For example, a key physiological requirement is that the right and left ventricular stroke volumes are approximately equal in a heart beating at a limit cycle, as the blood pumped by the right ventricle into the pulmonary circulation must match the amount pumped by the left ventricle into the systemic circulation. This balance is not achieved in this study.*

We thank the reviewer for identifying the stroke volume imbalance. We acknowledge the physiological requirement that, in a steady-state limit cycle, the right ventricular stroke volume must approximately equal the left ventricular stroke volume. However, since our model does not explicitly prescribe volumes, to achieve this, we would need to either explicitly tune active tension for the left and right ventricles separately, such as done in *https://www.frontiersin.org/journals/physiology/articles/10.3389/fphys.2021.716597/full* or develop a more sophisticated circulatory model and employ a multistep procedure that sequentially tunes circulatory dynamics, passive mechanics, and active contraction, such as done in *https://www.biorxiv.org/content/10.64898/2025.12.11.693778v1.full*. Both of which are beyond the scope of this paper.

We note that, despite the absence of explicit RV calibration, the RV volumetric measures and pressures remain within physiological ranges, suggesting that the coupled biventricular mechanics are broadly plausible. As such, we have noted this limitation in our discussion section, and sign-posted to other studies where the stroke volume match is achieved.

> *(7) The conclusive claim that "the study paves the way towards credible electromechanical cardiac Digital Twins" is not supported. The model exhibits non-physiological behavior, requires unsupported parameter alterations (such as a 10-fold active stress scaling), and does not represent a digital twin, as model data are drawn from various unrelated, non-patient-specific sources.*

We thank the reviewer for this comment, which gives us the opportunity to clarify our use of the term 'digital twin'. A cardiac digital twin is envisioned as a patient-specific computational model of the heart, personalised from multi-modal clinical data and continuously updated to support diagnosis, prognosis, and treatment planning. This is a transformative goal for precision cardiology that the field is actively working towards, with credible, systematically validated electromechanical models as its essential foundation. To our knowledge, no published study in cardiac electromechanical modelling has simultaneously fulfilled all three requirements, and it is for this reason that the community often refers to the 'digital twin vision' rather than its realisation.

The primary contribution of this manuscript is the framework: a systematic application of ASME V&V40 standards to a fully coupled electromechanical model, spanning electrical, mechanical, and haemodynamic biomarkers in a single study. The model evaluation presented here is an example application of that framework. Importantly, the framework is not designed to certify a model as complete, but to provide a transparent audit of current capability by identifying where confidence is established and where further development is needed. In this sense, the limitations surfaced through this evaluation are themselves a contribution: they define open problems and priorities for the field.

We have added a definition of the digital twin concept and the roadmap towards its realisation to the introduction and have updated the language throughout the manuscript to consistently reflect the distinction between the framework contribution and the model evaluation. We maintain that this transparent approach represents a meaningful step towards the digital twin vision.

The specific limitations of the current model implementation are addressed in detail in the relevant sections of this response and in the updated manuscript, where we have substantially strengthened the verification and discussion components.

> *Conclusion:*
>
> *Overall, this reviewer considers that the study requires a major revision, including improvements in numerical methods, modeling choices, and checks for physiological behavior. Nevertheless, the provided tables with averaged values from the UK Biobank and the presented validation strategy could be valuable to the research community.*
>
> ***Reviewer #2 (Public review):***
>
> *The authors present an interesting study on calibrating and validating a biventricular cardiac electromechanical model. This is an important contribution, but some questions remain about the quantitative validation and verification aspects of the study.*
>
> *Major comments:*
>
> *(1) The title and paper stress the importance of validation on several occasions. However, the actual validation performed is limited to the section in lines 427-439. Furthermore, it is entirely qualitative, making assessing the model's quality difficult. Most of the paper is focused on sensitivity analysis, which is also interesting but unrelated to validation. Can you include a quantitative comparison with deformation biomarkers? E.g., spatially quantify strain differences between simulation and in vivo data, or overlay the current configuration of the geometry with MRI in various views, and calculate a displacement error norm.*

We thank the reviewer for this comment.

We have strengthened the quantitative aspect of the validation by reporting the peak simulated strain values for each component and comparing them against the physiological ranges compiled in Table 2. Specifically, the simulated peak strains were: $E_{ff} \approx -0.20$, $E_{cc} \approx -0.15$, $E_{rr} \approx +0.15$, and $E_{ll} \approx -0.23$. These show broad agreement with the *in vivo* reference ranges from Moulin et al. (2021), noting that the reference ranges are derived from a cohort of 30 subjects and therefore represent a relatively narrow population sample. Shortening strains (fibre and circumferential) are in good agreement, while radial strain is underestimated. We have noted this as a limitation. We have also indicated that a further validation would include a fully quantitative spatial comparison, such as a displacement error norm or voxel-wise strain difference map. This would require access to the raw image data and patient-specific geometry registration, which is beyond the scope of the current study.

> *(2) You mention the ASME V&V40 standards throughout your paper. Yet, you only address the "second V" validation, ignoring the "first V" verification. How did you ensure that your computational models are implemented correctly?*

Thank you for raising this point. We have now included a section on model verification to the manuscript at where we perform benchmarking simulation using the Land (2015) passive inflation benchmark. We also provide a mesh subdivision analysis of the final calibrated model. Additional verifications and previous sensitivity analyses using the same numerical scheme with idealised ellipsoid geometries are also referenced in the verification section, to provide additionally confidence.

> *(3) All parameters discussed in this publication are physical parameters. What is the sensitivity of your model outputs concerning computational parameters?*

Numerical analyses for the Alya solver used in this study has previously been published in works including Levrero et al (2021), which performed sensitivity analyses in a truncated ellipsoid geometry, and Santiago et al (2018), which demonstrated mesh convergence in a cantilever. We have updated the manuscript to point the reader to these studies.

> ***Recommendations for the authors:***
>
> ***Reviewer #1 (Recommendations for the authors):***
>
> *Major concerns:*
>
> *(1) Active stress scaling:*
>
> *The initial value for T_ref appears to be 120kPa * 10, which would be ten times the literature value fitted to human contraction data. Additionally, Table 2 lists a range of [1200-2400], which is 10 to 20 times the literature value.*
>
> *This discrepancy suggests that other model parameters, model assumptions, or the numerical scheme may be inadequate. In contrast, similar calibrations using comparable models (ToRORd-Land) in other works, such as Strocchi et al. [29], yielded T_ref values close to the literature value.*

We thank the reviewer for this comment. As discussed in our response to the public review comment 3a, the elevated T_ref scaling warrants explanation.

We note that Strocchi et al. use a four-chamber geometry include atrial mechanics and a different pericardial constraint, any of which could contribute to differences in the required T_ref scaling. The elevated scaling in our model likely reflects a combination of factors including the absence of poro-elastic behaviour, simplifications in pericardial constraint, and the lack of atrial mechanics, rather than volumetric locking alone. We have added text to the discussion acknowledging this more explicitly and have flagged planned additional benchmarking of the dynamic orthotropic scheme as future work.

> *(2) Non-physiological results, see Figure 1:*
>
> *In a healthy heart, RV stroke volume should approx. match LV stroke volume. This is clearly not the case in Figure 1B, where the RV EF is also notably low at 35%.*
>
> *Consequently, the study fails to reproduce healthy pressure-volume loops, undermining its claim to create a credible cardiac electromechanical digital twin. Hence, also the "Question of interest" posed in line 206 must be answered with a clear "No".*
>
> *Matching stroke volumes should be a primary calibration goal.*

We thank the reviewer for this comment. We agree that stroke volume balance is an important physiological criterion, and we have added it explicitly to the framework criteria in the updated manuscript, noting that our current model evaluation does not satisfy it. This is precisely the kind of transparent appraisal the V&V40 framework is designed to produce: a systematic accounting of which criteria are met and which require further development. A framework that only gets applied to models that pass all criteria would be selection-biased and less informative to the community.

However, we respectfully disagree that the question of interest must be answered with a clear 'No'. We draw the reviewer's attention to the quantities of interest defined in the paper, which are predominantly left ventricular biomarkers, reflecting the intended scope of the calibration framework. The framework successfully reproduces these defined quantities of interest, and the LV pressure-volume loops, strain, volumes and ejection fraction are all

within physiological ranges and well-matched to reference data. These quantities of interest were selected based on their clinical implications in cardiac diseases, as detailed in Table 3.

We agree that stroke volume balance is an important physiological requirement for a fully calibrated biventricular model, and we have strengthened the future work and limitations section accordingly.

> *(3) Inadequate numerical framework:*
>
> *(a) Monodomain model: The geometries from Rodero et al. [25] have an average edge length of 1mm. It is known that such a coarse resolution leads to inaccurate EP results. It is not mentioned if the authors refined that geometry to an appropriate resolution or used an Eikonal model to mitigate this issue.*

As explained earlier, our ECG simulations are robust against coarse mesh resolutions since we use an Eikonal solution to prescribe the activation times on the endocardial surface, as performed in Camps et al. (2024), and we tune the diffusivity parameters in the model such that the correct conduction velocities are reached. We have added a figure in the appendix of this manuscript to show that by increasing the mesh resolution by one subdivision, we get virtually identical ECG simulations. While this mesh resolution may not be sufficient for simulations of more complex behaviour, such as re-entry and fibrillation patterns, it is sufficient for this study. We have noted this in the methods section.

> *(b) Material law:*
>
> *- recent publications show that an unsplit deformation gradient for the anisotropic contribution is beneficial to reduce locking effects, see, e.g., Gueltekin et al. Computational Mechanics 63, no. 3 (2019): 443-53. https://doi.org/10.1007/s00466-018-1602-9.*
>
> *- K_ct is a penalty parameter to enforce some degree of incompressibility. Results are highly dependent on the grid size and the finite element formulation due to locking effects.*
>
> *As the authors write: "In our simulations, we saw that the LVEF was strongly sensitive to changes in the incompressibility of the tissue (Kct), such that an increase in compressibility of the myocardial tissue helped to increase LVEF." Which exactly points to the issue of locking effects.*
>
> *So an option would be to use a finer grid or a more adequate numerical scheme with quadratic finite elements, as eg. in [5] Fedele et al., or [6] Gerach et al,. or stabilized elements as in Karabelas et al. CMAME 394 (2022) https://doi.org/10.1016/j.cma.2022.114887.*
>
> *Overall, this does not point to "limitations in using ex vivo tissue measurements to represent in vivo function" but to limitations in the numerical setup. In fact, with an adequate numerical scheme, the simulations should be largely insensitive to the choice of this penalty parameter K_ct. See, e.g., Karabelas et al. above, where the authors varied K_ct from 650kPa to infinity (representing an incompressible material), and there is no visible influence on the PV loops.*

We investigated this point using the Alya solver, and we found that the mesh resolution did not alter the LVEF, and our benchmark simulations against Land (2015) did not show the existence of the volumetric locking issue that the reviewer refers to. It is possible, however, that such an effect exists in the elastodynamic orthotropic framework but not in the incompressible and transversely isotropic framework that the Land (2015) benchmarks were set up in. Future analyses could focus on performing additional benchmarking against more

recent elastodynamic benchmarks, such as presented in Arostica (2025). We have updated the limitations text in our manuscript to reflect this and to cite relevant literature on this issue.

> *(4) Boundary conditions:*
>
> *"This was a simplified version of the method [28], which uses an exponential decay formulation at the 'edge' of the pericardial constraint rather than a step function": I don't really see this in the cited work [28] which gives a spatially varying Robin-type boundary condition at the whole epicardium (i.e. regional scaling of normal springs stiffness based on image-derived motion from CT images) and not only at the edge.*
>
> *This is motivated by the fact that the pericardial tissue is in contact with various organs of different material properties. Not using spatially varying pericardial parameters is a limitation that might lead to non-physiological deformations, see also Pfaller et al. Biomechanics and Modeling in Mechanobiology 18 (2019): 503-29. https://doi.org/10.1007/s10237-018-1098-4.*

We thank the reviewer for this point and we have corrected the manuscript accordingly. To clarify: our implementation applies a uniform Robin spring constraint along the majority of the epicardial surface with zero constraint at the base, which is conceptually similar to Strocchi et al. [28]. The key difference is that Strocchi et al. use a smooth gradient transition from uniform constraint to zero constraint near the base, whereas our implementation uses an abrupt step transition. We acknowledge that a smooth spatially varying transition would more accurately represent the frictionless pericardial contact and have noted this as a limitation in the manuscript with reference to Pfaller et al. [41].

> *Also check:*
>
> *- line 117: Gamma_valve_epi is introduced but not used. Was there any boundary condition defined on this valve plane?*
>
> *- the third equation, maybe (0,T] missing.*
>
> *- line 120: epicardium instead of endocardium.*

These errors have been corrected in the updated manuscript. No boundary conditions were applied on the epicardial surface of the valve plugs, the reference to gamma_valve_epi has been removed.

> *(5) Reference geometry:*
>
> *The choice to scale the mesh to a lower volume for the unloading procedure seems questionable. This approach does not ensure that the reloaded mesh aligns with the mesh derived from image data. As a result, the geometry used for the simulations is no longer truly patient-specific.*
>
> *This mismatch is a significant limitation, as there are established methods available to achieve a proper unloaded configuration, as, e.g., in*
>
> *Marx et al. Journal of Computational Physics 463 (2022): 111266. https://doi.org/10.1016/j.jcp.2022.111266, and*
>
> *Regazzoni et al. Journal of Computational Physics 457 (2022): 111083. https://doi.org/10.1016/j.jcp.2022.111083.*

As our study aimed at creating a framework for calibration and validation in data-scarce scenarios such as it is often the case in the clinical context, using a compilation of multi-modal data from difference sources, rather than a specific method of personalisation, we did not feel it appropriate to invest significant energy to identify a patient-specific resting

geometry, but rather felt that it was important for the resting geometry to fall within population values in terms of diastasis volume. We have clarified this issue in the manuscript and softened claims to Digital Twins in this study. The limitation has been addressed in the updated manuscript, and future work could further address this point.

> *(6) Calibration procedure:*
>
> *There are apparent flaws in the calibration procedure, or it is not described in sufficient detail.*

We thank the reviewer for raising this point and we have substantially revised the calibration description in the manuscript to clarify the rationale behind each step.

> *(a) Step 1: "Sample..." Why? kws and Cal50 are not the most significant parameters in the sensitivity analysis. Kct is a penalty parameter dependent on the numerical framework as described above; "ejection pressure threshold" was never mentioned, is it "P ejection LV" in Table 2? Aiming just for the highest LVEF might neglect non-physiological responses to parameter changes.*

While kws and Cal50 are not the single most significant parameters for LVEF in isolation, they were grouped in Step 1 because they affect both LVEF and peak systolic pressure simultaneously through cross-bridge cycling rate and residual active tension, making it necessary to sample them jointly rather than sequentially. Kct was included because myocardial compressibility affects wall thickening and therefore stroke volume. The ejection pressure threshold is P_ejection_LV in Table 1 and has now been described explicitly in the methods section. Regarding the concern about non-physiological responses: the action potential duration and active tension were monitored throughout calibration and verified to remain within physiological ranges, as now noted in the manuscript.

> *(b) Step 2: As systolic pressure is directly dependent on arterial resistance for a 2-element Windkessel model, a uniform sampling approach might not be the best choice here.*

We acknowledge that uniform sampling may not be the most efficient approach for Step 2. However, since arterial resistance influences not only peak systolic pressure but also stroke volume and therefore LVEF, a more targeted approach focusing solely on pressure matching could compromise the LVEF achieved in previous steps. Uniform sampling allowed us to select the value that best balanced both quantities simultaneously.

> *(c) Step 3: The authors mention in line 527: "A four-fold increase in GCaL caused an eight-fold increase in cellular active tension peak". An increase in active tension peak results in higher LVEF. So this step is likely to yield the upper boundary of the GCaL interval.*

The reviewer is correct that Step 3 tends to yield a high GCaL value. This was intentional — GCaL was used as a last resort to achieve physiological LVEF after Steps 1 and 2, since the model consistently undershot the target. The upper boundary of the sampled GCaL interval corresponds to a two-fold increase, which remains within the physiological variability bounds applied in previous studies. The resulting action potential duration was verified to remain within physiological ranges.

> *(d) Step 4: Why again k_ws? It is not the most significant parameter in the SA.*

kws was resampled in Step 4 not to increase LVEF further, but to specifically target peak ejection rate and dP/dtmax, which were not adequately matched after Step 3. kws is the dominant parameter affecting these ejection dynamics biomarkers in the sensitivity analysis. Resampling at this stage allowed fine-tuning of ejection dynamics while maintaining the LVEF achieved in previous steps.

> *(e) Step 5: As far as I can tell, the "diastolic volume change parameter" was mentioned the first time here.*

The diastolic volume change parameter C_pLAV has now been described in the methods section in the Phase 5 passive filling description, where it appears as the inverse of the penalty term controlling the rate of return to diastasis volume in the left ventricle.

> *The whole calibration procedure seems to aim for the highest LVEF, and final values of the calibration parameters are not given.*

We note that the calibration procedure does not aim solely for the highest LVEF. As described above, the sequential strategy targets multiple quantities of interest in order of clinical importance: LVEF, peak systolic pressure, peak ejection rate, and peak filling rate, with each step designed to improve a specific subset of biomarkers without compromising those already matched. The final calibrated parameter values are reported in Figure 1F of the revised manuscript.

> *(7) Novel features in this paper are actually scarce. A way more advanced calibration strategy with a whole heart model, emulators, and also the ToRORd-Land model was already presented in the study by Strocchi et al. [29]. The calibration to ECGs was presented by some of the same authors in Camps et al. [15], and the analysis of cellular effects was already published in several studies by the same group and in other publications, e.g., by the groups of Severi et al.*

The systematic compilation of credibility criteria spanning ECG morphology, pressure-volume characteristics, strain and displacement represents a novel contribution in itself, providing the field with a reusable evaluation framework. Furthermore, the present study is designed to yield mechanistic insight into how parameters at different scales influence both electrical and mechanical outputs simultaneously. This goal was not tackled in previous publications, which covered individual components, including ECG calibration in Camps et al. [15] and global sensitivity analysis with whole-heart models in Strocchi et al. [29] with no ECG consideration.

Thus, the work by Camps et al. on ECG calibration was purely electrophysiological and did not investigate the influence of mechanical or haemodynamic parameters on ECG morphology in a fully coupled electromechanical framework. While the effect of mechanical parameters on ECG has been explored by others (e.g. Favino, 2016), this has not previously been examined alongside the relative importance of cellular, mechanical and haemodynamic parameters on pressure-volume characteristics within a single coupled framework. While Strocchi et al. present an emulation strategy, they did not address ECG biomarkers. This distinction is now stated explicitly in the introduction, where we position the present study relative to Camps et al. and Strocchi et al.

> *(8) How could the calcium sensitivity Cal50 have such a drastic effect on diastolic function, i.e., filling and end-diastolic volume? As far as I understand from the description, the simulation starts with Phase 0 (loading), Phase 1 (atrial filling), and then in Phase 2, electrical activation ensues and active contraction develops, see also the section starting in line 165. Based on this description, I would expect the end-diastolic volumes to be identical across all Cal50 values. Or are the PV loops shown actually limit cycles established over simulations with multiple beats? This point wasn't explicitly clarified in the manuscript.*

Calcium sensitivity (Cal50) affects not only systolic active tension development but also diastolic residual active tension, i.e. the degree to which the muscle remains partially activated at end diastole. Higher Cal50 values increase this residual tone, effectively stiffening the myocardium during diastolic filling and reducing end-diastolic volume. This

mechanism is well established as a contributor to diastolic dysfunction in heart failure [88]. We have clarified this in the manuscript and also clarified that the PV loops shown are single-beat simulations, not limit cycles, with the end-diastolic volume determined by the prescribed filling pressure alongside the passive and residual active stiffness of the myocardium.

> *Minor concerns:*
>
> *(9) Line 29: The values provided: LVEF of 51%, EDV of 110 mL, and ESV of 50 mL are inconsistent. If these values are all related to the LV, the calculated LVEF should be approximately 54.55%, not 51%.*

The values quoted in the original abstract were rounded approximation, this has been corrected to report EDV=105 mL and ESV=51 mL, which are consistent with the simulated LVEF of 51%.

> *(10) "Electromechanical cardiac Digital Twins have had broad applicability ..."*
>
> *Many of the cited works here are not true "Digital Twins" but rather static, non-patient-specific models of cardiac electromechanics. In some cases, the geometry may be derived from patient data, but this alone does not qualify the model as a digital twin.*

This sentence in the introduction has been rephrased as 'Electromechanical cardiac models have had broad applicability...'. Furthermore, as stated earlier, we have removed explicit claims of Digital Twin from the paper while retaining the fact that this study provides a significant step towards rigorous credibility assessment of the high-fidelity electromechanical models that make Digital Twin construction possible.

> *(11) While in the abstract and the conclusion, the authors mention "uncertainty quantification", it is mostly a sensitivity analysis that was performed in the paper.*

We have updated the text to say 'sensitivity analysis' where appropriate in the abstract, results, and conclusion, and replaced 'uncertainty ranges' with 'variability ranges' throughout. However, since the sensitivity analyses were performed over biologically informed ranges derived from population variability in the literature, the results are informative about how uncertainty in model inputs propagates to uncertainty in simulated biomarkers. We have therefore retained the framing of sensitivity analysis as a first step towards uncertainty quantification in the abstract and conclusion, and have added a clarifying sentence to the methods to this effect.

> *(12) Line 98: As far as I can tell, the conduction velocity assigned to the endocardial surface - intended to mimic the Purkinje fiber network - is never specified. In the section beginning at line 294, only the transmural conduction velocities are reported.*

The endocardial conduction velocity has been specified in the methods section: Purkinje-myocardial junctions were modelled using a fast endocardial activation layer with isotropic conduction velocity of 300 cm/s.

> *(13) Line 198, Table1:*
>
> *(a) "21/02/2025 11:09:00 AM" on two occasions is maybe not intended*

This has been removed.

> *(b) For easing up comparisons, units should be consistent between the initial value and the literature ranges, e.g., PV control parameters, heart rate.*

Units have been made consistent between the initial values and literature ranges throughout Table 1.

> *(14) Line 232: "... have already been used to calibrate and validation ...".*

This has been corrected.

> *(15) Line 279, Table 2: This table of variability ranges is not entirely clear and could be improved:*

Table 2 has been combined with Table 1 such that the variability ranges sit next to the literature values, for ease of comparison.

> *(a) "21/02/2025 11:09:00 AM" is maybe not intended.*

This has been removed.

> *(b) use of units should be improved; sometimes it's given in the first column, sometimes in the second column (arterial resistance, compliance), then for k_epi it should be either kPa or kPa/cm.*

Units have been made consistent and the units for k_epi has been added in Table 1.

> *(c) units should also be consistent throughout the paper, e.g. in Figure 1 E arterial resistance is Barye.ms/mL while in Table 2 it is mmHg.ms/mL.*

Barye has been removed and replaced by corresponding kPa values throughout the manuscript. This was in the original manuscript since the Alya simulation software were in units of cm, s, g, Barye.

> *(d) it is also not clear how variability ranges were chosen; e.g., for arterial compliance,e literature ranges are 0.2-2.73 while the chosen range is [0.1,0.2].*

The previous ranges were chosen to achieve better LVEF. We have now updated the variability ranges to be purely based on literature values and updated the sensitivity analysis results. The ranges are now presented in Table 1 alongside the literature values for ease of comparison.

> *(e) For Kct, the initial value in Table 1 is 5000kPa, the literature values are between 10 and 3333, and then the variability range is [10,500]? I guess there is a typo in one of these values.*

This has been corrected in the new Table 1.

> *(f) Table 1 and 2 are in parts redundant.*

Table 1 and 2 have been combined into a single new Table 1.

> *(15) Line 290: It should be uvc_l for the longitudinal coordinate.*

This has been corrected.

> *(16) Line 388, Table 3, regarding values for pressure volume from reference [49]:*
>
> *(a) the number of participants is 800, including males and females; not only females, see also Table 12 https://jcmr-online.biomedcentral.com/articles/10.1186/s12968-017-0327-9/tables/12*
>
> *(b) why using female values here while having mixed sex for most of the others? Because the model is female?*

The reviewer is correct that reference [49] reports values from a mixed-sex cohort of approximately 800 participants. We used the female-specific values from Table 12 of that

reference because the biventricular mesh used in this study was derived from a female subject, making sex-matched reference values the most appropriate comparison. This has been clarified in the manuscript.

> *(17) Figure 5: What is Jup; why did you choose 0.93 x Jup as reference? Also in Figure 4, why did you use 0.93 x GCal as a reference?*

J_up refers to the SERCA<sup2+ reuptake current, which has been relabelled as SERCA throughout the manuscript for consistency. The reference value of 0.93× was used because the sensitivity analysis sampled parameters uniformly between 50% and 200% of baseline using a fixed number of samples, and no sample fell exactly at 1.0×. The closest sampled value was 0.93×, which was therefore used as the reference. This has been clarified in the figure caption.

> *(18) Line 377: The link to the GitHub repository does not work.*

This link has now been made publicly available.

> *(19) Line 397, Table 3: for the sake of completeness, all abbreviations should be included: e.g., SVL, ESP, EDV, ESV are not included.*

This has been written out in full in the new Table 2.

> *(20) Tick marks in many figures are not readable, e.g., Figure 5 and all the Figures in the appendix.*

Tick mark sizes and line widths have been increased across Figures 4, 5, and all appendix figures. The figures have been replotted and updated in the revised manuscript.

> ***Reviewer #2 (Recommendations for the authors):***
>
> *Minor Comments:*
>
> *(1) The provided GitHub link https://github.com/jennyhelyanwe/Alya_input_setup/ does not work, potentially because the repository is private. It would be nice to see the repository during the review.*

This link has now been made publicly available.

> *(2) Table 3: Can you include the simulation outputs obtained for validation (with an error indication)? This would summarize the validation that's currently spread out over the results section.*

A new Table 3 has been added to the manuscript under the validation section, summarising the simulated values for all deformation and strain biomarkers alongside their reference ranges. The calibration and validate datasets are now reported separately in Tables 2 and 3, respectively.

> *(3) Figure 1: Add axis labels to all plots.*

Axis labels have been added to all subplots in Figure 1 in the revised manuscript. Simulated pseudo-ECG amplitudes are normalised and therefore dimensionless.

> *(4) Figure 2: Simulated and in vivo strains with exactly the same axes (size, range, ticks) and add grid lines to enable a comparison. Add the mean values of each in the other plot.*

The revised Figure 2 now includes the median *in vivo* strain values from Moulin et al. overlaid as a red dashed reference line on the simulation panels, enabling direct visual

comparison. The simulated mean could not be overlaid on the *in vivo* panels as the original Moulin et al. figure data are not publicly available for replotting. Exact axis matching was not applied as this would cause some simulated curves to fall outside the visible range, obscuring the model behaviour.

> *(5) Figure 3: The thickness (relative importance of the connections) is impossible to see in this plot. Instead of having gray background connections, remove them entirely below a certain threshold. Make the differences in thickness more pronounced or introduce a continuous color scale for the magnitude of the positive or negative correlation. Alternatively, you could rank the parameters from least to most important in each subfigure A-D and/or provide some numeric values.*

Figure 3 has been updated. All non-significant connections ($|r| < 0.6$ or $p > 0.05$) have been removed entirely, and gray lines have been removed in each subfigure, making the significant relationships clearer. A continuous blue-to-red colour scale has been applied to indicate the direction of correlation (blue: negative, red: positive), with line thickness proportional to the magnitude of the r-value.

> *(6) Figure 3 and Table 2: Why were material parameters b, bf, bs, and bfs omitted from this study (but included a, af, as, and afs)?*

The b parameters (b, bf, bs, bfs) appear in the exponent of the Holzapfel-Ogden constitutive law and are strongly coupled to the a parameters (a, af, as, afs), which carry units of kPa. In practice, the b parameters can only be reliably identified from *ex vivo* multiaxial stretch experiments, whereas the a parameters can be estimated from clinical imaging data. Since our study focuses on calibration and validation in a clinical data setting, we included only the a parameters in the sensitivity analysis, consistent with previous personalisation studies.

> *(7) Figure 4: What do the dotted lines represent?*

The dotted lines in Figure 4E highlight the increased longitudinal shortening with increasing GCaL, showing the basal plane moving towards the apex while the apical position remains unchanged due to the pericardial constraint. This has been clarified in the figure caption.

> *(8) Figures 4, 5, A2-45: Can you use a continuous color scale (e.g., from blue to red) for low to high parameter uncertainty?*

A continuous blue-to-red colour scale has been applied to Figures 4, 5, and all appendix figures A2–A6, where blue indicates the lowest parameter value and red indicates the highest. A colour bar has been added to each figure for reference.

https://doi.org/10.7554/eLife.106555.2.sa0